Neutron-converter backfills for microstructured semiconductor neutron detectors

by

Daniel Louis-Patrick Watson

B.S., Missouri University of Science & Technology, 2014

A THESIS

submitted in partial fulfillment of the requirements for the degree

MASTER OF SCIENCE

Alan Levin Department of Mechanical and Nuclear Engineering
Carl R. Ice College of Engineering

KANSAS STATE UNIVERSITY
Manhattan, Kansas

2023

Copyright

Abstract

Micro-structured Semiconductor Neutron Detectors (MSNDs) emerged in the 2010s as a commercially available neutron detector with ideal size, weight, and power (SWAP) traits and inherently high gamma rejection ratios. The MSND technology was repurposed with double-sided devices (DS-MSNDs) and pixelated imaging devices of both single- and double-sided variants (X-MSND and X-DSMND). The upper limit of neutron detection efficiency with this technology is constrained by both the microstructure geometries of the semiconductor diodes and the properties of the neutron-reactive backfill. Methods to increase the packing fraction of ^{6}LiF were investigated, leading to a sonic-tamping process regularly achieving >40% packing fraction results. Backfilled wafers were inspected for damage with leakage current measurements and showed no significant deterioration from the weighted-sonicated process.

Parallel investigations sought to use alternative materials and methods to backfill neutron converter materials. Solvents of lithium fluoride were identified and their capabilities to dissolve and precipitate lithium fluoride showed no success, indicating previous publications instead observed surfactant-like behaviors. Efforts to backfill metallic lithium within the trenches revealed that low thermal contraction lithium-passivation conformal coatings would need to be applied to the silicon microstructured diodes before filling. The synthesis of lithium hydroxide during successive heated aqueous particle washing cycles was revealed, and a particle treatment process was conceived, producing microparticulate ^{6}LiF optimized for mechanical backfilling with high measured zeta potential and low agglomeration. Finally, lithium peroxide was investigated as an alternative backfill due to the high atomic density of lithium; methods indicated that solvent-driven precipitation within the devices could yield packing fractions above 15% for this material.

Table of Contents

List of Figures v
List of Tables ix
Acknowledgements x
Dedication xi
Preface xii
Chapter 1 - Neutron Detection 1
Chapter 2 - Microstructured Semiconductor Neutron Detectors (MSNDs) 5
Chapter 3 - Neutron Reactive Backfills 10
Chapter 4 - Backfilling Techniques 18
Chapter 5 - Experimental Results 32
Chapter 6 - Conclusions 60
Appendix A - C++ Automation of Iterative MCNP Calculations 66

List of Figures

Figure 1-1. Neutron converter cross sections [50] 1
Figure 1-2 - Bragg Curve for neutron converter fragments in silicon from TRIM [3], using 1000 particle histories. The 2.73 MeV triton emission from the ^{6}Li conversion maintains the highest range in silicon. 3
Figure 2-1. Neutron conversion in a MSND backfill and subsequent energy transfer into the backfill and semiconductor substrate. Reactions A, B, C and D indicate that significant energy transfer occurs within the backfill or above the detector, decreasing the intrinsic detection efficiency. Reactions E and F illustrate an ideal scenario where the end of the Bragg curve terminates within the substrate, producing the largest quantity of charge. 6
Figure 2-2. Cross-section view of a MSND backfilled with ^{6}LiF. 7
Figure 3-1 - A Pulse-height spectra generated from MCNP6 in ^{6}LiF at a 60% mass density, approximating a 60% packing fraction. The intensity represented is normalized per thermal neutron impingent upon the detector area, known as the intrinsic efficiency..... 11
Figure 3-2. SEM image of microparticulate ^{6}LiF 14
Figure 4-1. Electron Beam Evaporative Coating of LiF onto 30 µm Diameter 20 µm Deep Cylindrical Holes [3]..... 18
Figure 4-2. MSND Trench Parameters for Conformal Coatings 20
Figure 4-3. Diagram of Dynamic Light Scattering Setup in ALV Hardware and Software with Representative Intensity and Autocorrelation Display from ALV Software. 27
Figure 4-4 - Bounded boxes achieving the minimum perimeter, and thus sampling the min-feret diameter from the shortest leg of each bounded rectangle..... 28
Figure 4-5. Layout of Malvern Zetasizer ZSP with Emulated Signal and Autocorrelation from Zetapotential Measurements, without Multiple Scatter Angle Measurements. 28
Figure 4-6 - Particles with negative surface charges of differing densities. Increased charge density on surfaces causes reduced agglomeration and increases dispersion stability. 29
Figure 4-7 – An arbitrary particle with a negative surface charge, attracting positively charged ions or positive molecule poles. 30

Figure 4-8- Malvern Instruments Zetasizer cuvette front and side view. Gold-plated electrodes pictured allow for the inducing of particle motion with an applied alternating current and voltage power supply. Laser scattering occurs at the bottom. 31
Figure 5-1 - Solubility of LiF in EC as reported [33] 32
Figure 5-2. LiF before (left) and after (right) boiloff within ethylene carbonate 34
Figure 5-3 - Thermal ramp-down of EC, supersaturated with LiF. Slow cooling proceeded in an effort to drive particle coarsening phenomenon in preference to nucleation..... 35
Figure 5-4 - LiF-backfilled MSND upright in a beaker with heated EC:LiF mixture. Diode trenches are exposed to the solution and the temperature drop is measured. 35
Figure 5-5 - Bare MSND upon destruction from reacting with molten Lithium, within an inert glovebox..... 37
Figure 5-6 - ^{6}Li foil hand-pressed into empty MSNDs at 140 ˚C on a hot plate with stainless steel roller..... 37
Figure 5-7 - A Parylene-N coated wafer, sandwiched between parchment paper (cellulose), which was pressed with a manual roller above 200 ˚C on a hot plate. Lithium was successfully melted without violent reactions. 38
Figure 5-8 - A Parylene-N coated wafer (Figure 5-7), upon uncovering revealed visual damage to the underlying MSNDs. 38
Figure 5-9 - The backside of an empty MSND wafer segment, coated in Parylene-N, fracturing from thermal stresses in the polymeric film. 39
Figure 5-10 - ParyFree coated MSND wafer, with molten lithium being pressed against the trenches by a silicone manual roller..... 40
Figure 5-11 - Particle size distributions following agitation by pipette within a quartz cuvette, for the first 4-5 minutes after agitation. RDT MSND production ^{6}LiF (thought to be ripened) is measured on the left and purchased LiF measured on the right..... 41
Figure 5-12 - Dynamic Light Scattering Measurements, Sampling Particle Size Distributions After 5 Minutes of Settling of Microparticulate ^{6}LiF. At this point, it was certain that particle ripening was negligent and the nomenclature “washed/treated” was purposed to denote production-ready material. 41
Figure 5-13 - Polydisperse micro/nano-particulate ^{6}LiF, sampled from RDT MSND production stockpiles. ^{6}LiF particles were sputtered with 20 nm gold to improve micrographs..... 42

Figure 5-14 - LSW (from Lifshitz, Slyozov, and Wagner) ripening kinetics of LiF in H_2O, with the diffusion coefficient sampled from DLS and surface energy of 570 erg cm^2 [47]. 43
Figure 5-15 - ^{6}LiF particulate ground for 150 seconds from open-air castings 44
Figure 5-16 - Manually measured ground ^{6}LiF (left) from 4-1-21, and automated image-analysis measurements (right) from the same micrograph, both in units of µm. 44
Figure 5-17 - Manually measured ground ^{6}LiF (left) from 5-28-21, and automated image-analysis measurements (right) from the same micrograph, both in units of µm. 45
Figure 5-18 – Zeta potentials measured for ^{6}LiF with various particle treatments, using a Malvern Zetasizer Nano ZSP. Ratios at the end of the labels denote a decrease in dispersion concentration to test samples for multiple-scattering influence. Values are displayed as absolute but were all measured negative. 47
Figure 5-19 - Leakage currents measured in -3V (reverse bias) for selected diodes on each wafer. Each wafer was processed in a mixture of 0.33L methanol to 10g of treated material for 1-hour of sonication. Note the Ammonium hydroxide-washed wafer reflects 3 diodes that passed leakage current tests (<25nA in reverse bias, with >100µA in forward bias) after processing, a result of cleaning the bonding pads. Devices not achieving >100µA in forward bias are denoted "n/c", indicating poor electrical connection between the electrical probe and the diode, through the bond pad. 49
Figure 5-21 - Leakage current measurements in -3V (reverse bias) for empty MSND wafer backfilled with acetic acid-treated ^{6}LiF. Wafers were sonicated for 1h with 333 mL methanol to 10g treated ^{6}LiF. Following sonication, the wafers were dried, weighed, and then packed by hand with methanol-wetted treated ^{6}LiF, using silicone brayers. 50
Figure 5-20 – Leakage current measurements in -3V (reverse bias) for empty MSND wafer backfilled with ^{6}LiOH-treated ^{6}LiF. Wafers were sonicated for 1h with 333 mL methanol to 10g treated ^{6}LiF. Following sonication, the wafers were dried, weighed, and then packed by hand with methanol-wetted treated ^{6}LiF, using silicone brayers. 50
Figure 5-23 - Layout of a 1500 mL borosilicate beaker prepared to perform the weighted-sonicated method of backfill. 52
Figure 5-22 - A Quantrex 650H sonicator with polymer sheet cut to hold 6x 1500 mL beakers in suspension within the sonicated water bath [5]. Positions are referenced 1-6, as their locational effects were determined to alter the outcome of backfills. 53

Figure 5-26 - Packing fractions for the 2nd VLSI trial. Locations in this diagram reference the overhead locations in the sonicator. 54
Figure 5-25 - Packing fractions for the last 2 wafers of the first VLSI run. Locations in this diagram reference the overhead locations in the sonicator. 54
Figure 5-24 - Packing fractions for first VLSI run with weighted-sonicated backfill. Locations in this diagram reference the overhead locations in the sonicator. 54
Figure 5-27 - Dendritic growth of Li_2O_2 within the trenches of what was an MSND. The dendrites at the top of the device limited the precipitation of Li_2O_2 within the active volume of the device. 57
Figure 5-28 - Simulated efficiencies for MSNDs using a pulse-height tally (F8) within MCNP6. Note that the upper yields on efficiencies are dictated by the LLDs. 6LiF, the overall best backfill candidate, performs exceptionally across most packing fractions, is electrically insulating, and does not react chemically with any device materials or moisture. 58
Figure 5-29 - Simulated efficiencies for the double-sided variants of the MSND (DS-MSND and X-DS-MSND). These devices exhibit similar packing-dependent efficiency behavior to MSNDs but utilize the double-sided design to reduce neutron streaming through the fins of the microstructures. 59

List of Tables

Table 2-1. Micro-Structured device parameters (all lengths in µm)..... 5
Table 3-1. Backfill candidate material properties for 95% atomic enrichment Li-6..... 12
Table 4-1. Selected Routes to ALD of LiF [23, 24, 25] 19
Table 4-2. Conformal Coating Thickness, Time, and Packing Fraction for MSNDs..... 22
Table 4-3 - Solubility of LiF in H2O [44] 24
Table 5-1 - EC solvated recrystallization of LiF in LiF-backfilled MSNDs. 32
Table 5-2 - Packing fractions for the highest-performing treated particulate, with manual packing. 52
Table 5-3 - Packing results for treated ^{6}LiF without manual packing. 52

Acknowledgements

I would foremost like to acknowledge my advisor, Dr. Douglas McGregor. His patience and guidance have instilled upon me the teachings necessary to achieve my academic and professional goals. Secondly, I would like to recognize my committee members, Dr. Takashi Ito and Dr. Gurpreet Singh. I am most grateful to the sponsor of my research, Dr. Steve Bellinger, whose expertise and wisdom were crucial to the investigation performed herein. Dr. Taylor Ochs and Luke Henson's helpful discussions, guidance, and thoughts gave me the background I needed to solve the problems this research presented.

I am thankful to have been assisted by the members of SMART Lab: Dr. Dan Nichols, Robyn Hutchins, and Jacob Terrel, all of whom assisted me with acclimating into laboratory, shared their technical expertise, and made me feel welcome to the team. I wish to also acknowledge the staff of RDT, Radiation Detection Technologies, who were very supportive when I needed their assistance.

I present this work with the appreciation of Dr. Christopher Sorensen and his research group for their contributions to the measurement of particles with dynamic light scattering. Dr. Tej Shrestha of the KSU Nanotechnology Core provided insight to the zeta potentials observations and assistance with equipment usage.

I am most gracious for the support of my parents, James and Mari Watson. Without their unending encouragement and patience throughout my life, I am certain I would never have achieved this.

Dedication

I wish to dedicate this thesis to my late aunt, Arlene Avakian. We all love and miss you.

Preface

This thesis was intended to communicate the investigation of an engineering challenge, how to produce a neutron converter backfill in micro-structured semiconductor neutron detectors that exceeds current standards in one or more criteria: manufacturability, intrinsic thermal neutron detection efficiency, and process yields. This thesis is designed to provide individuals who possess a basic scientific skillset an expedient & concise background on the challenge explored before discussing the specific physics and advanced methods implemented herein. This thesis does not discuss (in-depth) the fundamental science surrounding nuclear interactions, chemistry, semiconductors, microfabrication, or radiation detectors. If readers wish to understand microstructured semiconductor neutron detectors further, review of the following doctoral theses are highly recommended: Dr. Steve Bellinger, Dr. Ryan Fronk, and Dr. Taylor Ochs. In addition to these theses, a thorough background in radiation detection is provided within “Radiation Detection: Concepts, Methods, and Devices”, a comprehensive text by Dr. Douglas McGregor and Dr. Kenneth Shultis which this thesis has leveraged heavily.

Chapter 1 - Neutron Detection

Radiation detection is accomplishable if, and only if, at least 3 criteria are met: the radiation must interact with matter, the interaction must produce an observable effect, and the effect should be measurable [1]. This process is unambiguous for charged particles, which readily interact with the electron shells or nuclei of matter through coulombic forces. Photons are detected through the interactions they share with electrons (and less often nuclei), in which the electrons carry kinetic energy and undergo further coulombic interactions with matter. Neutrons, however, are challenging particles to detect as they carry no net charge and possess energy dependent absorption properties.

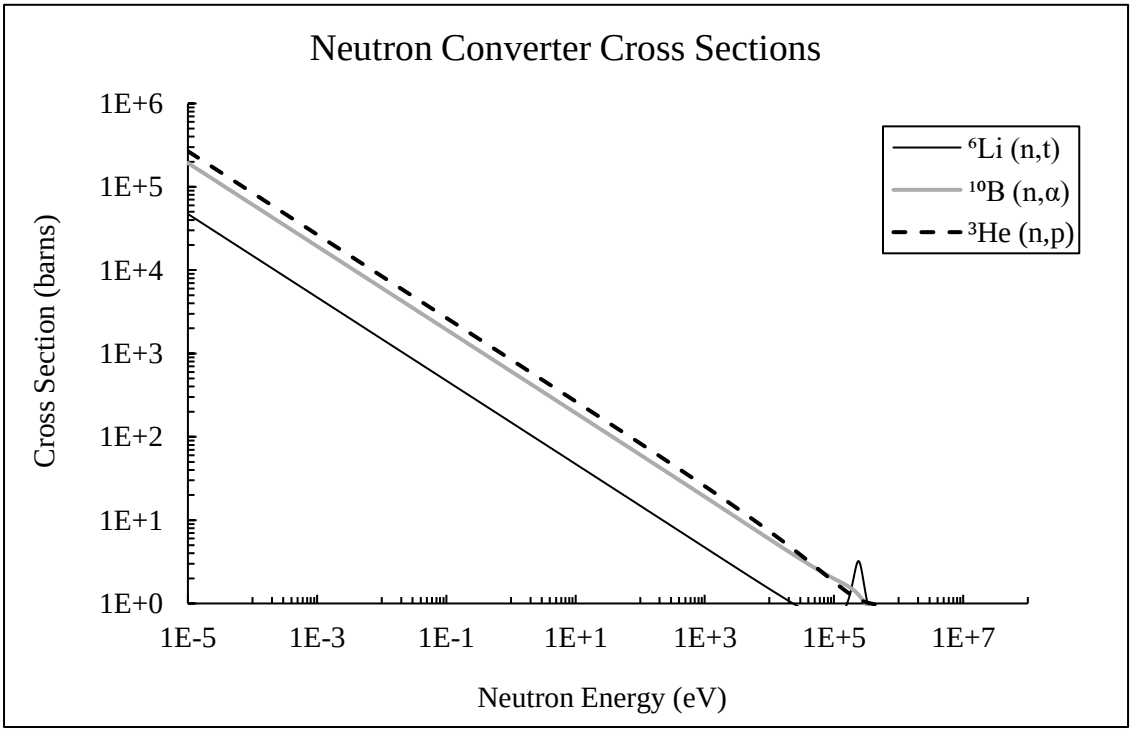

Figure 1-1. Neutron converter cross sections [50]

Detection of neutrons relies upon the observable effects they produce with matter. Furthermore, neutron interaction probabilities vary greatly with neutron energy, typically favoring lower energies with a few isotopes possessing uniquely large interaction probabilities (Figure 1-1). The average thermal energy of a neutron at 20 ˚C is calculated from multiplying the Boltzmann constant by the temperature, 293 K, and results in 0.025 eV. Neutrons at this energy are commonly referred to as "thermal neutrons". Because interaction probabilities favor the detection of thermal neutrons, the subject of this thesis lies completely with the detection of thermal neutrons.

Thermal neutron detectors primarily use ^{6}Li, ^{10}B, and ^{3}He to produce measurable effects from neutrons (i.e. "neutron converter materials"). These nuclei absorb neutrons and immediately fission, a reaction in which the nuclei fragment into small nuclei (each possessing kinetic energy). The fission fragments encountered for these small nuclides are consistent and purpose the nomenclature "(n,t)", "(n,α)", or "(n,p)" to denote triton, α, and proton production from the nuclear fission, respectively. Fission fragments transit from their origin into (or within) the detector. Their path through the detector liberates free charges, resulting from the strong coulombic interactions between the fission fragment and the detection media. A voltage-bias is used to drift the charges to either the anode or cathode. Their motion between the electrodes induces a current flow in a connected electronic circuit.

^{6}Li Conversion of Thermal Neutrons, 938b

$$^{6}_{3}\mathrm{Li} + {}^{1}_{0}\mathrm{n} \longrightarrow {}^{4}_{2}\mathrm{He}(2.05\ \mathrm{MeV}) + {}^{3}_{1}\mathrm{H}(2.73\ \mathrm{MeV}) \quad (1)$$

^{10}B Conversion of Thermal Neutrons, 3844b

$$^{10}_{5}\mathrm{B} + {}^{1}_{0}\mathrm{n} \longrightarrow \begin{matrix} 94\% & {}^{7}_{3}\mathrm{Li}^{*}(0.84\ \mathrm{MeV}) + {}^{4}_{2}\mathrm{He}(1.470\ \mathrm{MeV}) \\ 6\% & {}^{7}_{3}\mathrm{Li}(1.015\ \mathrm{MeV}) + {}^{4}_{2}\mathrm{He}(1.777\ \mathrm{MeV}) \end{matrix} \quad (2)$$

^{3}He Conversion of Thermal Neutrons, 5320b

$$^{3}_{2}\mathrm{He} + {}^{1}_{0}\mathrm{n} \longrightarrow {}^{3}_{1}\mathrm{H}(0.191\ \mathrm{MeV}) + {}^{1}_{1}\mathrm{H}(0.573\ \mathrm{MeV}) \quad (3)$$

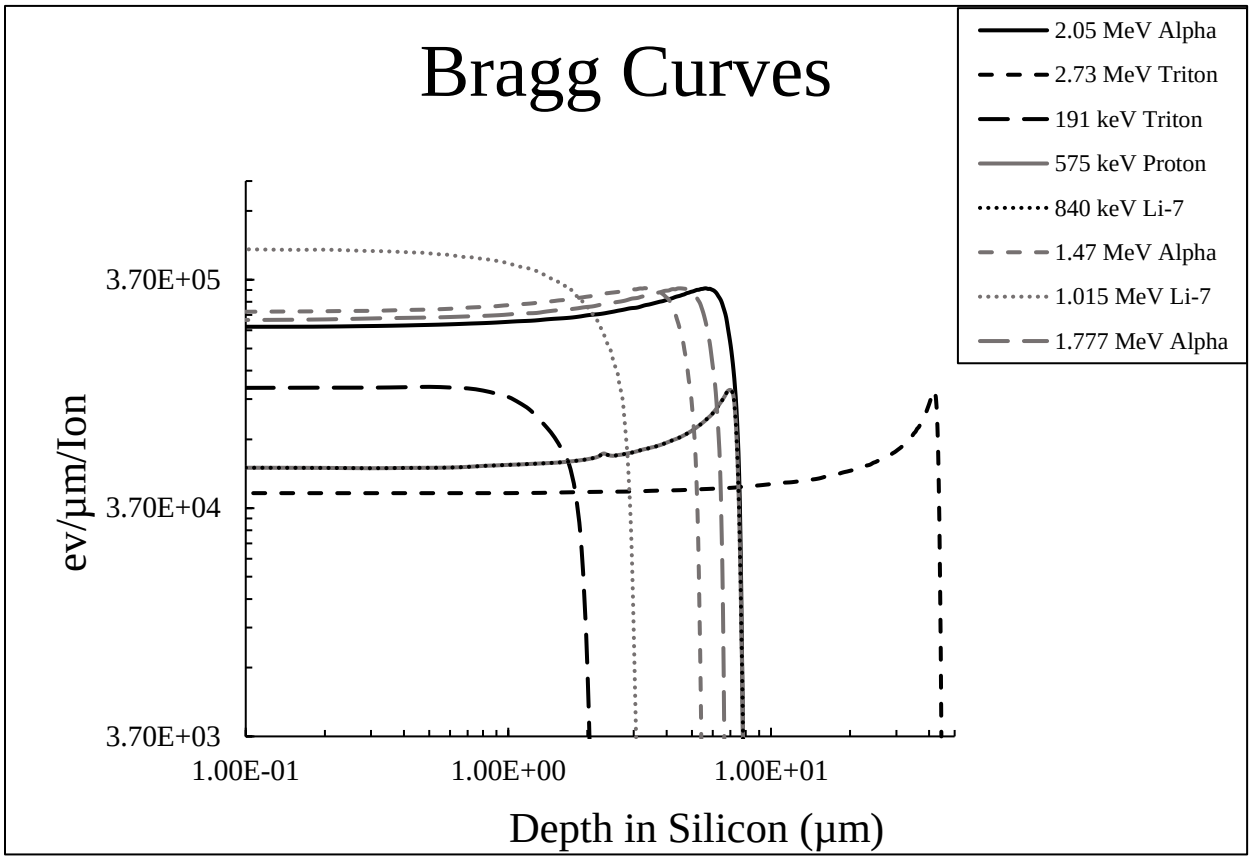

Figure 1-2 - Bragg Curve for neutron converter fragments in silicon from TRIM [3], using 1000 particle histories. The 2.73 MeV triton emission from the ^{6}Li conversion maintains the highest range in silicon.

For the case of semiconductors, electron-hole pairs are excited within the detector volume. Ions, interact with matter through coulombic forces and transfer energy with a well-known behavior [2], some of which are shown in (Figure 1-2). The semiconductor, by design, drifts the

electrons across the diode for collection at the anode with an applied bias voltage. The total charge (quantity of electron-hole pairs) coupled with the detector capacitance, produces an induced potential. The detector signals are subsequently measured and used for counting or spectroscopy.

Chapter 2 - Microstructured Semiconductor Neutron Detectors (MSNDs)

MSNDs emerged in the 2010s as an advanced commercial successor to the perforated neutron detector [3] [4] [5]. Simplistically, MSNDs are silicon diodes with micro-feature trenches etched partially through the substrate which are then backfilled with neutron reactive materials. These devices function better than planar diodes with neutron converter layers, due to the 2nd dimension in which neutron conversion produces charge within the detector substrate (Figure 2-1). The fins between trenches are doped to produce an internal bias and allow for greater depletion of the devices at lower reverse bias operations [5]. Standard MSND (and variant) trenches maintain high-aspect ratio (HAR) properties (Table 2-1).

Table 2-1. Micro-Structured device parameters (all lengths in µm).

Device	Trench Depth	Trench Width	Trench Length	Unit Cell Pitch	Trenches per Diode Side	Aspect Ratio
MSND	400	20	10000	30	333	20
DS-MSND	600	20	10000	30	333	30
X-DSMSND	450	28	15763	55	257	16

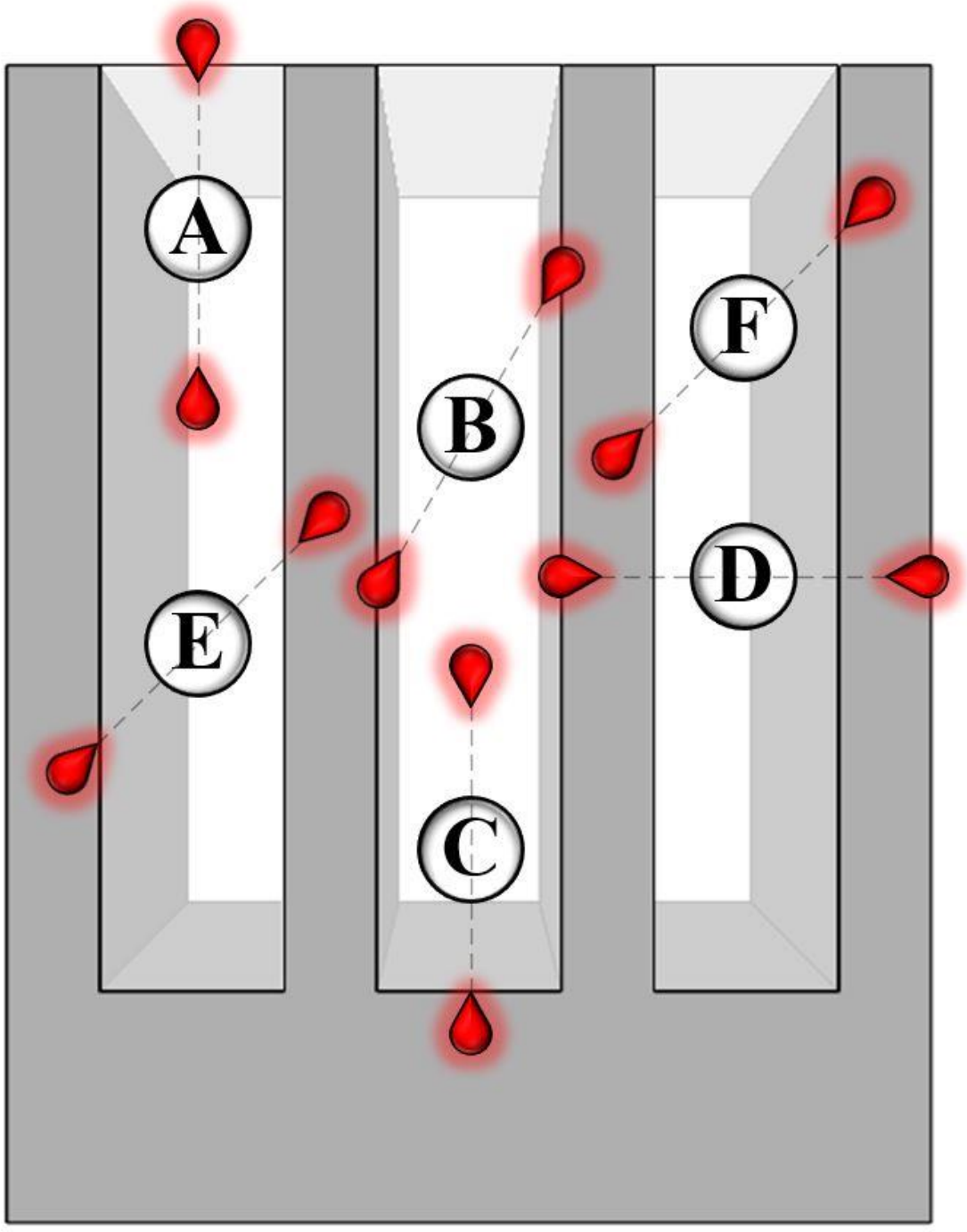

Figure 2-1. Neutron conversion in a MSND backfill and subsequent energy transfer into the backfill and semiconductor substrate. Reactions A, B, C and D indicate that significant energy transfer occurs within the backfill or above the detector, decreasing the intrinsic detection efficiency. Reactions E and F illustrate an ideal scenario where the end of the Bragg curve terminates within the substrate, producing the largest quantity of charge.

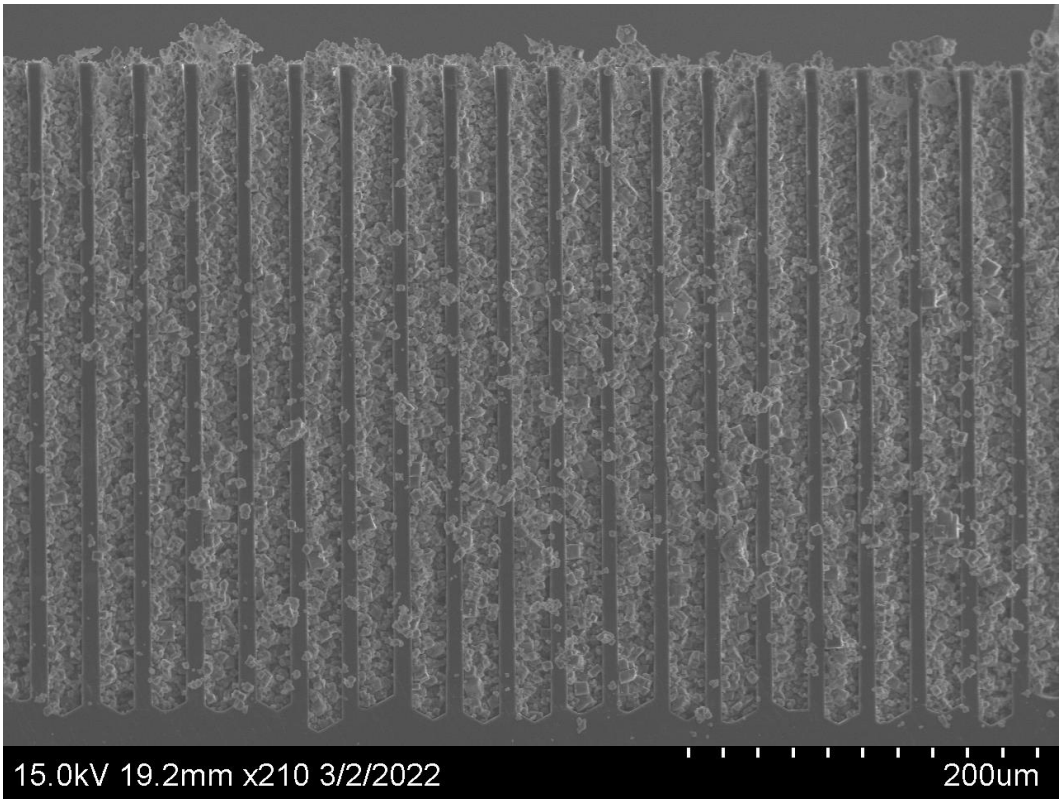

Figure 2-2. Cross-section view of a MSND backfilled with ^{6}LiF.

MSNDs provided a means of obtaining high intrinsic thermal neutron efficiency coupled with gamma-ray rejection (10^{6} neutrons/gamma detected [3]), due to the micro-structuring and chemical makeup of the substrate, silicon. By utilizing "low-Z" (low electron density) semiconductors, and by micro-structuring (producing a low effective density from the etching of trenches), the devices weakly interact with gamma-rays while producing a high-energy signal from neutron conversion with ^{6}Li.

Before the advent of MSNDs (and other perforated diode neutron detectors), semiconductor neutron detectors had consisted of bulk and planar devices. Bulk devices utilized neutron converters within the semiconducting compounds while planar devices detected neutron

conversion products, generated by a conversion coating, in a diode. Bulk neutron detectors have been challenging to produce as crystal growth methods require high temperature and pressure [1]. Bulk converter materials manufactured from boron can also change crystalline structures, resulting in reduced charge-collection efficiency and subsequent lower detection efficiency [1]. Bulk neutron detectors made from lithium-containing semiconductors have achieved thermal neutron detection efficiencies as high as 6.5% [6] and up to 24% for layered boron carbide heterojunctions [7]. Planar detectors have been shown to be limited in neutron detection efficiency by the ability to capture the neutron conversion products, a fundamental limitation imposed by the geometry of the detector. Layered planar diodes have been shown to substantially increase this efficiency, but only when arranged perpendicular to the radiation source. Limitations to the efficiency of a coated diode neutron detector have been determined [1], where single layers exceeded 25% thermal neutron detection efficiency while double layered devices exceeded 50% [8]. Micro-structuring neutron detectors was proposed as a means to capture all of the neutron converter products before [9]. By manufacturing high aspect-ratio filled devices, the limitation of thermal neutron detection efficiency can be realized by the packing capabilities of different neutron converter materials.

MSND (and DS-MSND) efficiencies had been studied before [3, 4, 5, 10] as a function of backfill packing fractions and trench geometries, utilizing MCNP to simulate neutron conversion and subsequent pulse generation within the semiconductor from alpha-particles and tritons; such simulations agreed with experimentally measured efficiencies for given packing fractions of ^{10}B and ^{6}LiF backfills, but did not investigate other materials. Other etching geometries (e.g. sinusoidal) presented fabrication challenges and ultimately a rectangular geometry was standardized within the development of the MSND. As packing MSNDs presented more difficulty

throughout the commercialization of the devices (and the development of their variants), an interest grew to confirm ^{6}LiF at the commercially reproducible packing fractions was optimal for thermal neutron detection and that other lithium-based candidate compounds did not produce improved conversion results within the MSNDs (and associated variants).

Chapter 3 - Neutron Reactive Backfills

Neutron reactive backfills before this research had mostly consisted of ^{6}LiF, an alkaline fluoride with one of the highest known atomic densities of lithium (Table 3-1). Previous efforts [3, 11] had asserted that the "ΣL product", the product of the macroscopic cross section for (n:t) reactions and the average path length of the resultant ions (alpha-particles and tritons), properly substantiated the choice for LiF as the backfill material. The "ΣL product" is a measure of the ability of a material to efficiently convert (absorb) neutrons while maintaining a high range of the converter products (minimal energy reduction of the ions as they traverse the backfill and enter the semiconductor). For a backfill consisting of N conversion ions, with ranges L in a backfill material of macroscopic conversion cross-section Σ_j, and M converter nuclides, the ΣL product can be determined (Eq. 4).

Calculation of the ΣL Product for Compounds

$$\Sigma \mathrm{L} = \frac{\sum_{\mathrm{i}=1}^{\mathrm{N}} \mathrm{L_i}}{N} * \sum_{\mathrm{j}=1}^{\mathrm{M}} \Sigma_j \tag{4}$$

A more thorough comparison of the backfill materials had not yet been investigated or published. A backfill performance study was performed for MSND, DS-MSND, and X-DSMSND geometries using MCNP 6.2. This study purposed the assumption that the different packing fractions could reasonably be modeled with varying mass (and atomic) densities of the converter material, occupying the trench geometry completely [5]. The simulation utilized a F8 tally within MCNP6, which emulates pulse-heights within user specified materials, divided into user specified energy bins (Figure 3-1).

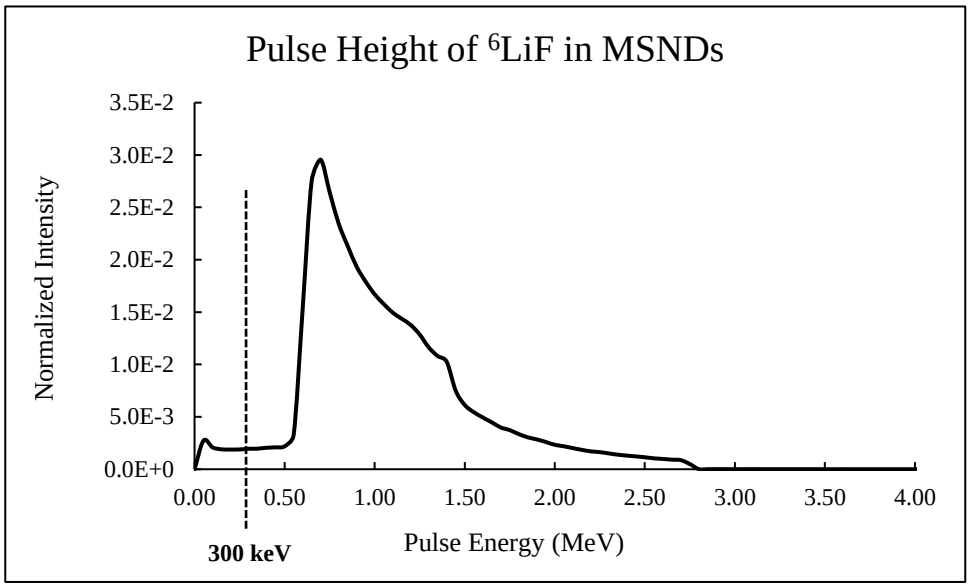

Figure 3-1 - A Pulse-height spectra generated from MCNP6 in ^{6}LiF at a 60% mass density, approximating a 60% packing fraction. The intensity represented is normalized per thermal neutron impingent upon the detector area, known as the intrinsic efficiency.

This tally, performed over the entire volume of the silicon substrate (which assumes the inaccurate complete charge collection efficiency throughout the sampled substrate), was executed iteratively for each backfill candidate material at varying densities with automation from a C++ script (Appendix A). The C++ script additionally provided the means to extract the relevant tally data from each MCNP (Monte Carlo N-Particle, a nuclear transport code by Los Alamos) output file with a convenient formatted output to a CSV (comma separated values) file. From the backfill performance study, the following lithium-based compounds were investigated (because of their atomic densities of lithium among other properties): metallic lithium, LiF, LiBr, LiCl, LiOH, Li_3N, LiI, and Li_2O_2.

Table 3-1. Backfill candidate material properties for 95% atomic enrichment Li-6

Backfill Material	Atomic Density of Li-6 (mol/cc)	Hazards (Health, Fire, Reactivity, Specific)	α Range (μm)	Triton Range (μm)	Macroscopic Cross Section (n,T) (Σ_a)cm	ΣL Product
Li	7.25E-02	3|2|2|~~Water~~	23.2	134.0	40.99	0.325 ± 0.004
LiF	9.65E-02	3|0|0|N/A	6.0	33.8	54.56	0.108 ± 0.002
LiCl	4.63E-02	2|0|0|N/A	8.4	49.9	26.20	0.076 ± 0.002
LiOH	5.79E-02	3|0|0|N/A	8.7	50.1	32.74	0.096 ± 0.001
LiBr	3.79E-02	2|0|0|N/A	8.5	47.2	21.42	0.060 ± 0.002
Li3N	1.04E-01	N/A|0|2|~~Water~~	10.1	59.2	58.75	0.203 ± 0.003
LiI	2.89E-02	2|0|0|N/A	8.4	48.3	16.36	0.046 ± 0.002
Li2O2	9.57E-02	3|0|2|Oxidizer	6.1	34.9	54.08	0.111 ± 0.002

Metallic Lithium

Metallic lithium when simulated for a 20μm:400μm trenched device achieved the highest maximum efficiency throughout the investigated materials. In its pure form, lithium maintains high ion transmissivity (23 μm for 2.05 MeV alpha-particles) without being compounded to parasitic neutron absorbers (which could foul the spectra with prompt or delayed auxiliary reaction products). Metallic lithium is a reactive alkali material, requiring passivation or encapsulation to protect the metal from degradation in atmosphere. Reacting lithium with the moisture in the atmosphere results in the formation of LiOH, that expands without any tendency to provide passivation to the underlying lithium (unlike typical metal oxides). Additional consideration to the chemical passivation of metallic lithium should include the diffusion of lithium within silicon, an n-type dopant that can change the semiconductor properties of diodes. Passivation and

encapsulation are also limited to lithium-compatible materials, requiring even further compatibility with process parameters of the finished devices (dry film encapsulation, dicing, wire-bonding, annealing, etc); the satisfaction of such requirements was investigated with the polymer parylene (types n and "parafree").

Lithium Fluoride

Lithium fluoride maintained the fourth highest performance across all backfill candidates. The material achieved a high efficiency with 39% for MSNDs with 300 keV LLD (lower-level discriminator) at a packing fraction of 0.75 for MSND geometry and held the third highest performance among the candidates up to a packing fraction of 0.4. Lithium fluoride is a stable alkyl halide with remarkably low solubility in all solvents except hydrofluoric acid (HF) [12, 13, 14]. The material is prepared from ^{6}Li-enriched metallic lithium (Eq. 5). This titration process produces ^{6}LiF micro crystals (Figure 3-2). Crystal sizes have been manipulated during nucleation and coarsening by the control of solution pH during titration with HF, with sizes between 30 nm [15] to 50 μm [16]. Furthermore, crystal size manipulation has been performed herein, using a "top-down" process in which large crystals are smelted and then ground into smaller irregular shapes.

The Synthesis of 6LiF

$$2^{6}\mathrm{Li} + 2\mathrm{H_2O} \longrightarrow 2^{6}\mathrm{LiOH} + \mathrm{H_2}$$
$$^{6}\mathrm{LiOH} + \mathrm{HF} \longrightarrow {}^{6}\mathrm{LiF} + \mathrm{H_2O} \qquad (5)$$

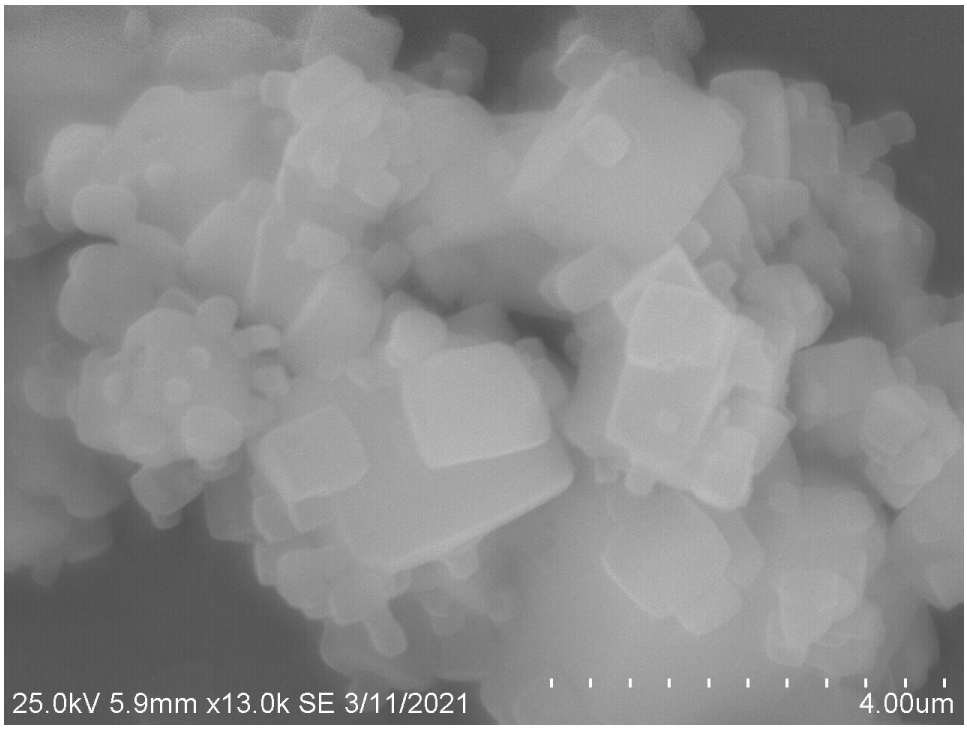

Figure 3-2. SEM image of microparticulate ^{6}LiF

Lithium Bromide

Lithium bromide (LiBr) is a binary halide possessing solvation properties in multiple solvents [14]. LiBr exhibits high solvation in water with a strong thermal dependence [17]. Common organic solvents (ethanol, acetone, methanol, and ether) are also capable of dissolving LiBr [18]. With a series of known solvents, a low neutron cross section of the halide (Bromine at 10.2 barns), low hazardousness, the concept of recrystallization was the motivation to investigate LiBr as a backfill material. Due to the hygroscopicity of the material, encapsulation would be a concern as the swelling of hydrated LiBr could potentially damage the diodes, especially if the backfill is not porous and instead consisted of large crystals contacting fins on both sides of the trench.

The synthesis of ^{6}LiBr

$$^{6}\mathrm{LiOH} + \mathrm{HBr} \longrightarrow {}^{6}\mathrm{LiBr} + \mathrm{H_2O} \qquad (6)$$

Lithium Chloride

Much like the solubility of LiBr, lithium chloride (LiCl) is soluble within methanol, ethanol, acetone, and water [19]. Thermal dependence coupled to the material solubility again provides the means to recrystallize this material into an entire wafer, lending to a VLSI compatible processing. Chlorine, however, is known to absorb neutrons (Cl at 49.7 barns) and emit gammas which causes the nuclei to become parasitic and foul the spectrum with a delayed signal (an undesired effect with radiation detection). While this effect is anticipated to remain minimal in comparison to thermal neutron conversion in a gamma insensitive device, it has yet to be quantified and will appear as a signal warranting discrimination with an aggressive LLD. Hazardousness for LiCl is similar to other lithium halides, where materials affect the nervous system when consumed.

The synthesis of ^{6}LiCl

$$^{6}Li_2CO_3 + 2HCl \longrightarrow 2\,^{6}LiCl + H_2O + CO_2 \quad (7)$$

Lithium Iodide

Lithium iodide has been used in scintillator neutron detectors with success (reported efficiency exceeding 80%) [20]. Iodine, with a thermal neutron absorption cross section of less than a single barn, exhibits no parasitic effect to the conversion of neutrons. As a MSND backfill the material exhibits low performance due to the low atomic density and reduced ion range (a result of the large halide in the binary compound). The material is prepared by reacting hydriodic acid with lithium carbonate or lithium hydroxide (Eq. 7). LiI can be readily dissolved in water, ethanol, methanol, acetone, and ammonium hydroxide [21]. The salt is remarkably hygroscopic, bringing concern that again the alkyl halide will expand once exposed to moisture. Lithium iodide, if purposed in MSNDs would require environmental passivation.

The synthesis of ^{6}LiI

$$^{6}\mathrm{LiOH} + \mathrm{HI} \longrightarrow {}^{6}\mathrm{LiI} + \mathrm{H_2O} \quad (8)$$

Lithium Hydroxide

Lithium hydroxide is the natural byproduct of exposing metallic lithium to a moist atmosphere (Eq. 9). The material is easy to produce, reacting cleaned (with xylene) metallic lithium with deionized water in a fume hood capable of safely removing the hydrogen gas. The triton and α neutron conversion products have deeper ranges in LiOH, at an average of 29.3 ± 0.1 μm but the lower molecular density yields an overall lower macroscopic cross section (and ΣL product) than LiF. Because of this, the material could only succeed as a backfill candidate if recrystallization techniques could provide higher packing fractions for which an upper yield to conversion efficiency rivaled LiF.

The synthesis of ^{6}LiOH

$$3\,{}^{6}\mathrm{Li} + 3\mathrm{H_2O} \longrightarrow 3\,{}^{6}\mathrm{LiOH} + 2\mathrm{H_2} \quad (9)$$

Lithium Nitride

Lithium nitride is a stable (at STP without carbon dioxide or moisture) alkyl nitride with the highest lithium atomic density. Nitrogen comprises the molecule with a total thermal neutron cross section of approximately 32 barns, much less significant than the 3 lithium nuclei each with a (n:t) cross section of this backfill candidate maintains the highest ΣL product throughout all proposed backfill candidates but has an unfortunate tendency to react violently with water, forming LiOH and ammonia (Eq. 10). This material would require satisfactory encapsulation with a moisture resilient coating compatible with both the semiconductor (low conductivity) and Li_3N.

Such a device would be reactive to water, if the encapsulation is breached, similar to modern lithium batteries. Without solubility in organic solvents, this material would require specialized in-situ synthesis from within the trenches (as metallic lithium under a pure nitrogen atmosphere) or dry mechanical pressing.

The Decomposition of Lithium Nitride

$$^{6}Li_3N + 3H_2O \longrightarrow 3\,^{6}LiOH + NH_3 \quad (10)$$

Lithium Peroxide

Lithium peroxide maintains a high atomic density of lithium (the third highest at 9.57E-02 mol cm^{-3}). The ΣL product for lithium peroxide is larger than that of lithium fluoride, indicating that the material parasitizes less neutron conversion product energies, producing more energetic signals upon conversion. Li2O2 can react with water to produce LiOH and O_2 (Eq. 11). This reaction can be avoided by complete encapsulation and chemical passivation as previously mentioned. Lithium peroxide is soluble in water but will react, which limits the ability to recrystallize Li_2O_2 within the trenches of MSNDs; recrystallization of Li2O2 in a backfilled LiF device, if possible, could provide a "boost" the diodes, as Li2O2 has a higher ΣL product than LiF and will not introduce parasitic effects or material with lower interaction cross-sections.

Decomposition of Li2O2 from Water

$$2\,^{6}Li_2O_2 + 2H_2O \longrightarrow 4\,^{6}LiOH + O_2 \quad (11)$$

Chapter 4 - Backfilling Techniques

Backfilling of high-aspect ratio microstructures is not a new goal in the scientific community; engineers have sought to produce gapless backfills in high aspect ratio (HAR) microstructures for micro electro-mechanical systems (MEMS) and dynamic random access memory (DRAM) technologies [22], extending the abilities of microfabrication. Previous methods in this area have used atomic layer deposition (ALD), chemical vapor deposition (CVD), plasma-enhanced CVD (PE-CVD), low pressure vapor condensation (LPVC), microfluidics, electroplating, and sonicated tamping of particulate. This thesis is focused on the following methods: conformal coatings, recrystallization, sonicated tamping, and mechanical pressing.

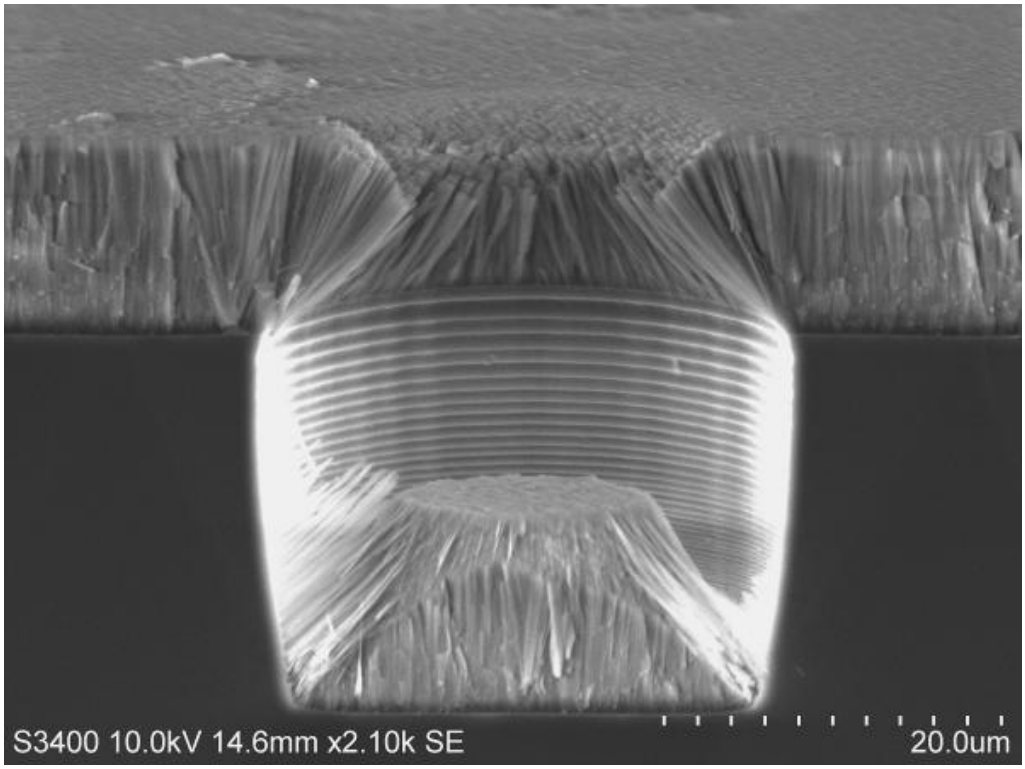

Figure 4-1. Electron Beam Evaporative Coating of LiF onto 30 µm Diameter 20 µm Deep Cylindrical Holes [3].

Conformal Coatings

Thin film coatings of LiF had been investigated before [3], where thermal evaporation and LPVC were used with limited success. Thermal evaporation, being a non-conformal (view factor) thin-film coating technique, resulted in the bridging of LiF across the trench fins (Figure 4-1), restricting further filling of the trenches [3]. LPVC achieved limited conformality and suffered the same bridging dilemma during processing [3]. A highly conformal technique would be necessary to fill the high aspect ratio microstructures of the MSND, which ALD is particularly suitable for.

Table 4-1. Selected Routes to ALD of LiF [23, 24, 25]

Precursor	Co-Reactant	Temperature (C)	Deposition Rate (Å cycle^{-1})
LiHMDS (Lithium bis(trimethylsilyl)amide)	HF-py (Hydrogen fluoride pyridine)	150	0.5
Lithd (Lithium tetramethylheptanedionate)	TiF4	325	1
Lithd (Lithium tetramethylheptanedionate)	Mg(thd)2 + TiF4 (Magnesium tetramethylheptanedionate)	325	1.4
LiOtBu (Lithium tertiary butoxide)	WF6	150-300	-
LiOtBu (Lithium tertiary butoxide)	MoF6	150-300	2.6
LiOtBu (Lithium tertiary butoxide)	TiF4	250	0.5
Lithd (Lithium tetramethylheptanedionate)	MgF2	275-325	-

ALD is a thin-film deposition process achieving high-conformality by coating specimens "one atomic layer at a time". The process proceeds with a precursor and co-reactant, two gases which when introduced into a vacuum chamber will chemisorb (chemically react with and bond) to the surface of a heated substrate. A precursor chemisorbs to the heated substrate, decomposing the metalorganic into components of a metal (adhered to the substrate) and an organic gas which

is evacuated into the downstream vacuum components. Following the precursor, a co-reactant chemisorbs to the surface, where in the case of LiF ALD a gaseous metal-halide decomposes, to form a strong bond between the halide and previously deposited alkyl metal. High conformality is attributed to the slow procession of coating as the vacuum chamber pulses precursor and co-reactant vapors into the chamber, each accompanied by "soaking" and "purging" steps in which the chamber pressure remains stable to promote diffusion of the gases into HARs and expels the remaining gases and reaction products from the reaction chamber, respectively.

The interest in investigating ALD for the backfill of MSNDs (and variants) appeared during the development of the X-DSMSND, a dual-sided pixelated neutron & gamma detector with integrated readout. The particulate backfills of LiF varied in packing fractions through the depth and length of the trenches in the microstructured devices, creating concerns with the range of device pixel sensitivities. Each device would need to be calibrated, purely as a result of the

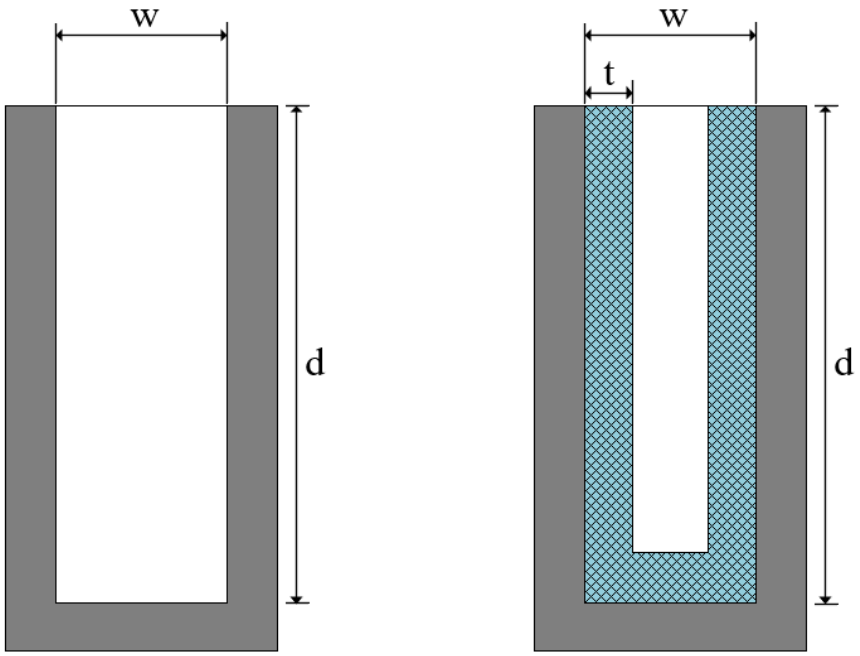

Figure 4-2. MSND Trench Parameters for Conformal Coatings

inconsistent packing fractions from diode-to-diode and wafer-to-wafer. Such methods (of calibrating each device) have been used for Anger Cameras [1], but an improvement to the consistency, control, and upper yields to X-DSMSND backfills would also serve as a significant manufacturing improvement to all MSND variants.

Initial calculations into the kinetics of ALD for a conformal backfill of a trenched device proceeded, using published growth rates of LiF [25] [26]. A simplified MSND trench of 20μm width with a 400 μm depth was purposed to determine the packing fraction as a function of conformal thickness - ignoring the 3rd dimension (length) of the trench, as the ratio of the film thickness to the length of the trench (typically around 1000 μm) would be negligible in this calculation. The packing fraction can be represented as a function of the width (w), depth (d), and conformal coating thickness (t).

Packing Fraction of a 2D MSND Trench

$$\mathbf{PF} = \frac{(\mathbf{w} \times \mathbf{d}) - (\mathbf{w} - \mathbf{2t})(\mathbf{d} - \mathbf{t})}{\mathbf{w} \times \mathbf{d}} \qquad (\mathbf{12})$$

Utilizing Eq. 12, in conjunction with the film growth rates (1.4 Å cycle^{-1}) the time necessary to achieve target packing fractions could be easily determined (Table 4-2). This calculation suggests that a coating achieving a 60% packing fraction would require 10 or more days of continuous processing for empty MSNDs. This long processing time would be subject to site power fluctuations, but equipment could be configured to record elapsed process duration and maintain vacuum during blackouts. In parallel, consideration was given to ALD of LiF on pre-packed (already backfilled) MSNDs. Particles have been coated with ALD in fluidized-bed systems [27], emphasizing slow deposition rates and the "flowing" of particles throughout the

chamber to achieve conformality. ALD of particles, stagnant within the trenches, would require more time to promote the diffusion of precursor and co-reactant gases within the labyrinths of backfilled trenches. With a significantly larger surface area in the trenches (up to an additional 2 cm^2 from a wafer with MSND geometry and 30% PF with 5 μm mean diameter cuboid particles) due to the stagnant particles, and the increased aspect ratio necessary to diffuse the ALD process gasses through, there currently exists no published experimental data on this proposed permutation of ALD backfilling.

Table 4-2. Conformal Coating Thickness, Time, and Packing Fraction for MSNDs

Time (days)	Film Thickness (μm)	PF
1	0.6	6%
2	1.2	12%
3	1.8	19%
4	2.4	25%
5	3.0	31%
6	3.6	37%
7	4.2	43%
8	4.8	49%
9	5.4	55%
10	6.0	61%
11	6.7	67%
12	7.3	73%
13	7.9	79%
14	8.5	85%
15	9.1	91%
16	9.7	97%

Further consideration of ALD requires the synthesis of ^6LiF precursors with SMART Lab and RDT stockpiles of metallic ^6Li. Precursors such as lithium 2,2,6,6-tetramethyl-3,5-heptanedionate (LiTHD) and lithium tertiary butoxide (LiO^tBu) could be produced within the SMART Lab facilities [28] [29], with LiO^tBu requiring additional glassware compatible with vacuum processes [29] to handle the volatile pyrophoric chemicals. Following the synthesis of enriched ^6Li precursors, the material would need to be handled and relocated into vacuum, thermal, and materials-compatible containers for the consumption within ALD where the material vessel would be vacuumed, heated, and vapors would be used within the ALD process.

Efforts to perform ALD of LiF within the MSND (and variant technologies) was ultimately abandoned due to multiple concerns; the process would require purchase or construction of expensive processing equipment, synthesis & handling of acutely toxic/hazardous materials, and would require significant processing time. Current backfill techniques, where LiF is mechanically packed into the MSND trenches, can consistently reproduce packing fractions within 30-40%. Justifying a new "exotic" process for backfilling with these considerations was determined infeasible.

LPVC

Previously, the backfill of MSNDs by low-pressure vapor condensation (LPVC) had been experimentally investigated [3]. MSND wafers were placed inside of a low-pressure chamber (100mTorr), in which vapors of LiF were produced (200 – 500 ˚C) and condensed onto the substrates that were cooled by a thermal feedthrough which coupled a copper cold finger to a liquid nitrogen cold trap. Permutations of this experiment yielded consistent results in which the devices were sealed with LiF upon minimal LiF condensation within the microstructures. This type of process is known to yield conformal coatings for other materials (i.e. parylene) but was unsuccessful with LiF.

Thermal Evaporation

Utilizing an electron-beam thermal evaporator, thin film coatings of LiF were grown on MSNDs [3]. Unlike ALD, CVD, or LPVC, the working principle behind evaporative coatings yields no semblance of conformality. The coatings form upon the condensation of low pressure (1E-6 Torr) vapors produced by heating LiF to 1020 – 1180 ˚C [30]. The vapors are expelled from

the surface and, due to the low pressure, move throughout the chamber without any significant collisions between the gaseous LiF molecules. The vapors, proceeding without diffusive behavior, are deposited on all surfaces "visible" to the material source. For HAR microstructures possessing sidewalls close to 90-degree orientations, gapless (complete) backfills with this methodology are not possible. Implementing wider angle sidewalls (>90 degrees) and rotary sample stages is known to improve the process, yielding gapless fills for microfeatures with low aspect ratio and scalloped walls [31].

Recrystallization

The concept of recrystallization is straight-forward, in that particle growth can be achieved from supersaturated solutions. This process would occur by decreasing the solubility or evaporating the solvent, leading to precipitation (or growth of previously backfilled particles) of the backfill material to form within the trenches. To proceed with a recrystallization backfill, the process would need to meet multiple criteria: nucleation would need to occur within the trenches of the MSND, particle coarsening (growth) would dominate nucleation in the transport of material from the solute phase, particle coarsening should occur evenly throughout the trench depth in order to avoid "bridging" or the effective sealing of the MSND trench, and the process

Table 4-3 - Solubility of LiF in H2O [44]

Temperature (C)	Wt.% (LiF / H2O)
23.7	0.132
25.4	0.133
30.8	0.137
40.5	0.137
50.1	0.142
51.2	0.141
60.2	0.145
71.4	0.148
81.8	0.150

would need to be implemented with materials & temperatures compatible with the MSND at this step in manufacturing (post doping).

^{6}LiF had been selected as the standard backfill material due to material stability, low conductivity, and high ΣL product. LiF, having a high lattice energy at 1036 kJ mol^{-1}, is insoluble in most solvents except hydrofluoric acid (an acid that etches silicon and is chemically incompatible with the devices at this step in the processing); ^{6}LiF does possess low solubility in water with a thermal dependence (Table 4-3). With a poor solubility in compatible solvents, ^{6}LiF backfill with recrystallization was entirely impractical as a 10% packing fraction increase would require 40 ml of water per diode (or 2 L per wafer) to evaporate with all precipitates ending within the trenches of the devices. Experimental investigation into water-based solvent recrystallization of ^{6}LiF had previously resulted in significant bridging of the devices (from agglomerated particles) and poor packing fraction yields. Other solvents were reported to have higher solubilities with ethylene carbonate at 12.9 g L^{-1} [32] at 60 °C and dimethyl sulfoxide at 0.58 g L^{-1} [14]. These solvents had not been investigated in prior work and, in theory, could accomplish a recrystallization backfill with ^{6}LiF. Other lithium halides had been considered in the backfill study (simulation) as their solubilities could lend their use to recrystallization backfills or "boosting" already filled MSNDs with additional neutron converter material; in addition to these other lithium halides, LiOH and Li_2O_2 were simulated as a conversion material as they also had strong solvents.

Mechanical Backfills

Previous work had leveraged mechanical methods to pack the MSNDs with microparticulate LiF, which was convenient as the production of LiF consistently resulted in

microparticulate LiF ranging in particle sizes between sub-micron and 10 μm. Mechanical methods such as isostatic pressing, centrifugal packing, sonicated dispersion tamping (weighted and unweighted), roll-pressing (with brayers commonly known as ink rollers), and combinations of one or more of those techniques [3] [4] [5] [33] had been investigated before.

Isostatic pressing, pressurized atmospheric loading upon a MSND wetted with a LiF slurry, had yielded packing fractions of 9 - 35% for MSNDs [5]. This process encountered the challenge of forming a gas-tight bond between a layer of wetted LiF and the MSND top-side and had not been experimentally investigated beyond the previous study [5]. With a high variance of packing fractions, the process was ultimately abandoned.

Centrifugal packing, by which MSNDs are placed into centrifuge cannisters with wet or dry LiF was previously investigated and implemented for the commercial backfill of MSNDs. Throughout the implementation of centrifugal packing, diode destruction increased, and the process was eventually replaced with a sonic-tamping technique [5].

Particle Size Effects

Previous experience yielded mixed packing results with different particle size distributions, testing micro and nanoparticulate LiF [5]. Further consideration to particle size distributions was given, with particle size measurements and modeling particle growth by Ostwald ripening mechanisms. Particle sizes for microparticulate LiF were measured with dynamic light scattering (DLS) and with image processing of scanning electron micrographs. Dynamic light scattering measurements of microparticles is made possible by the Brownian motion and settling behavior of

particles in fluids. By correlating the intensity of scattered light with an autocorrelation (a metric representing the similarity or correlation of time-dependent data throughout a measurement time domain), particle properties can be statistically expressed with Stokes-Einstein relationships (Figure 4-3 and Eq. 13). For particles with highly irregular shapes, an automated image-analysis technique provided an estimate of particle size distributions. The algorithm purposed a "min-feret" measurement technique, by which the smallest effective feature a particle could pass through in a single dimension was sampled (Figure 4-4). The process was initially performed with 3rd party macros in ImageJ (an open-source image analysis suite by the National Institute of Health), but eventually the features were implemented in the standard release of Fiji (an extended ImageJ release).

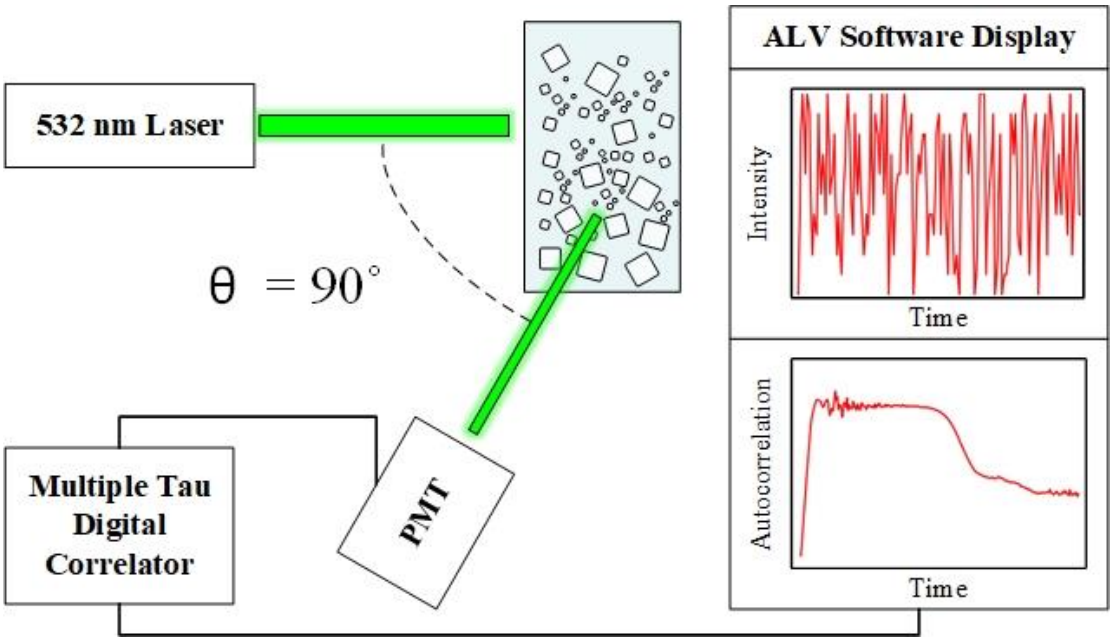

Figure 4-3. Diagram of Dynamic Light Scattering Setup in ALV Hardware and Software with Representative Intensity and Autocorrelation Display from ALV

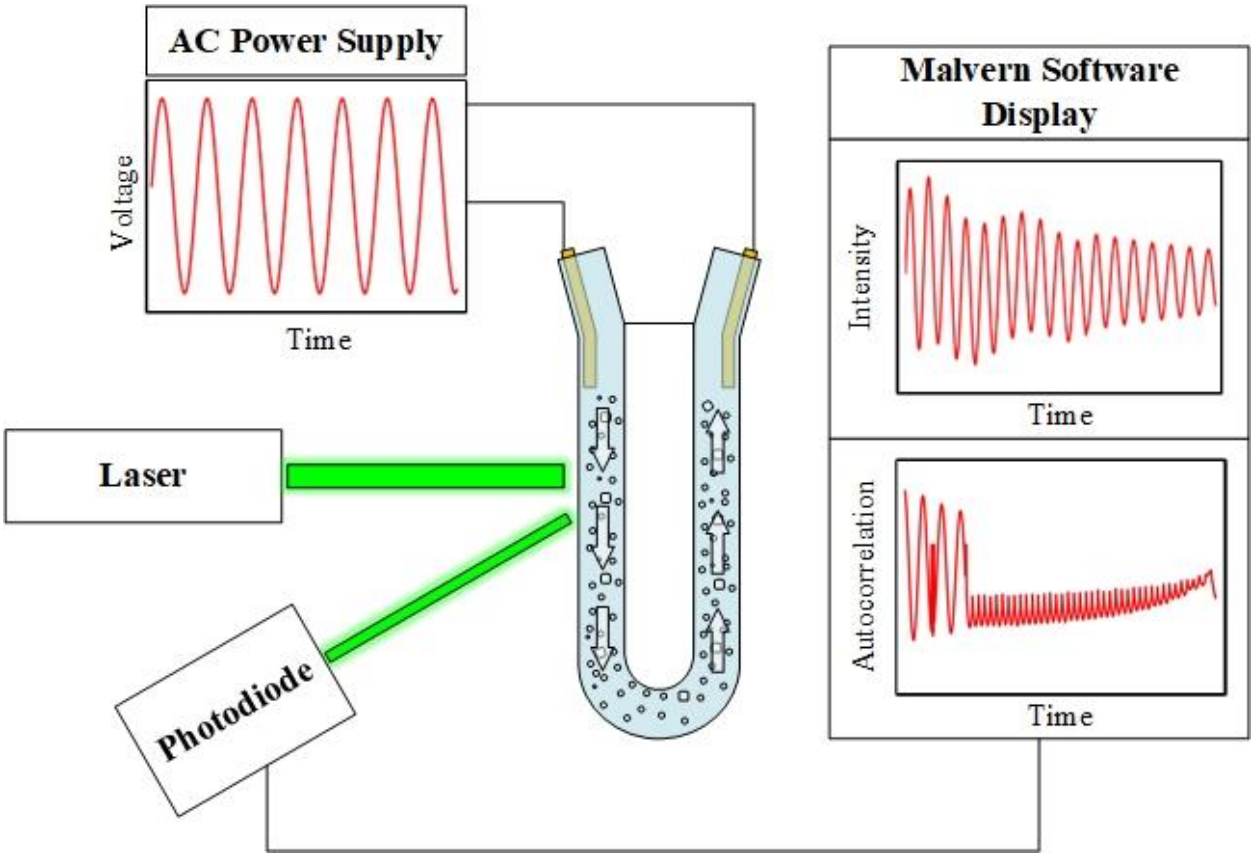

Figure 4-5. Layout of Malvern Zetasizer ZSP with Emulated Signal and Autocorrelation from Zetapotential Measurements, without Multiple Scatter Angle Measurements.

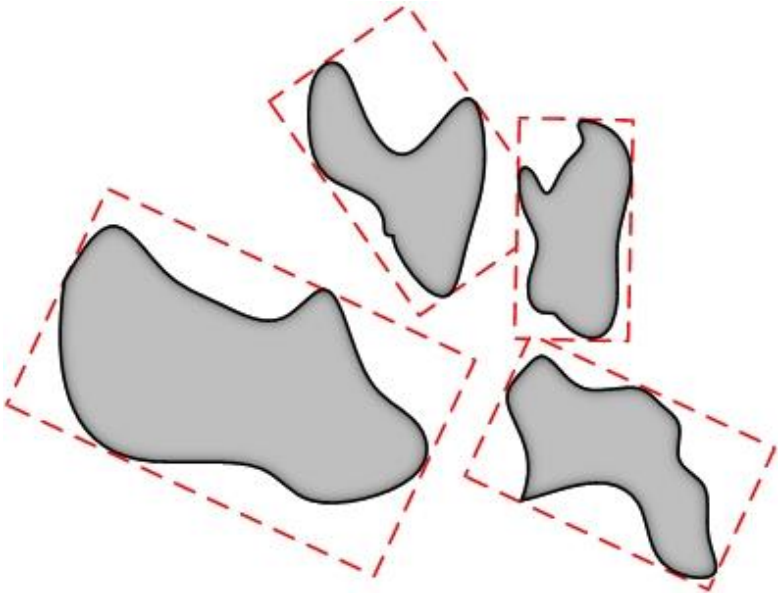

Figure 4-4 - Bounded boxes achieving the minimum perimeter, and thus sampling the min-feret diameter from the shortest leg of each bounded rectangle.

Einstein-Stokes Relation (Kinetic Theory of Particles)

$$D = \frac{k_B T}{6\pi\eta r} \tag{13}$$

Particle properties were studied, coupling experimental backfill results to the measured zeta-potential values from particle treatments. Particle setting is a well-characterized phenomenon, for which a known viscosity (η) fluid, tested at a specific temperature (T) can yield the relationship between the diffusion (D) of a particulate for a specific radius particle (r), using the Boltzmann constant (k_B). Zeta-potentials reveal the anti-agglomerating behavior of particles by measuring the movement of solid-in-liquid colloids through an alternating electric field and measuring the particle motion with DLS. Increased light scattering indicate increased particle motion and that particles carry a high surface charge, which would cause electrostatic repulsion and allow particles to overcome the Van der Waals forces that agglomerate them (Figure 4-6).

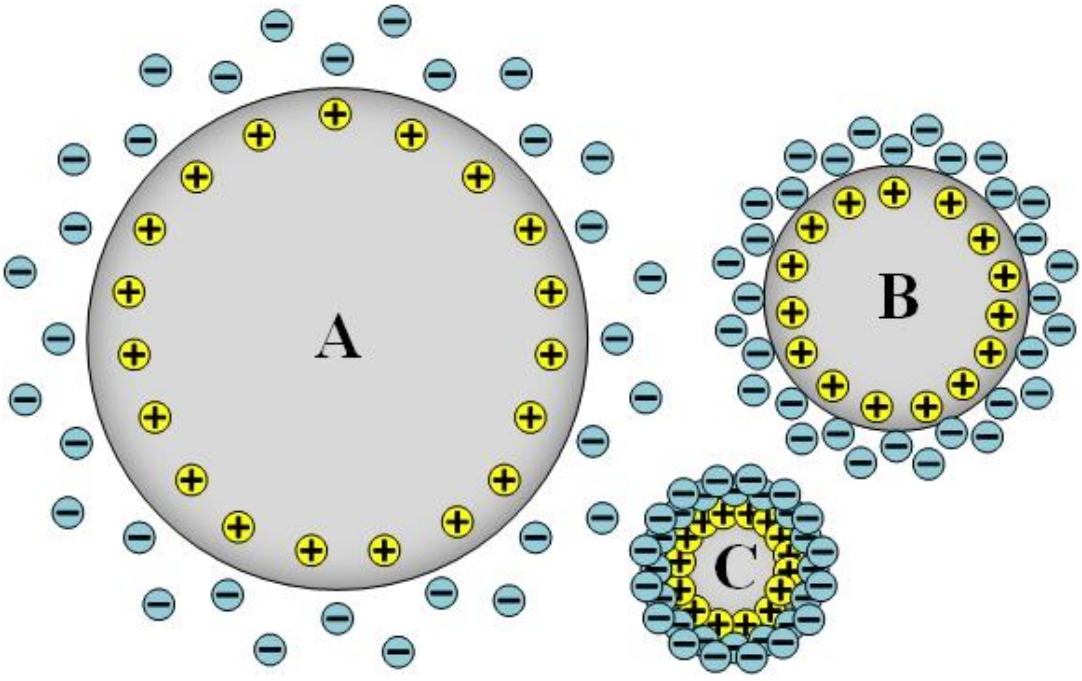

Figure 4-6 - Particles with negative surface charges of differing densities. Increased charge density on surfaces causes reduced agglomeration and increases dispersion stability.

In addition to investigations of particle growth ("bottom-up") mechanisms, a method to increasing particle size distributions by casting large ^{6}LiF crystals and grinding them into micro-powders ("top-down") was explored. Particles with larger sizes are predicted to agglomerate less due to their decreased ratio of surface area to material volume. Furthermore, larger (heavier) particles are expected to experience less stable dispersions in sonicated tamping, maintaining particle intimacy with the MSNDs and allowing vibratory motions translated from the horizontal plane to increase particle tamping into the trenches. These reasons motivated the investigation into the production (and use) of top-down ^{6}LiF particles. Previous castings of ^{6}LiF had been performed in open atmosphere but never purposed for this method of particle production. Concerns heating ^{6}LiF for casting in atmosphere arise due to the production of HF vapors and conversion of ^{6}LiF to ^{6}LiOH, motivating the production of ^{6}LiF ingots within inert atmospheres.

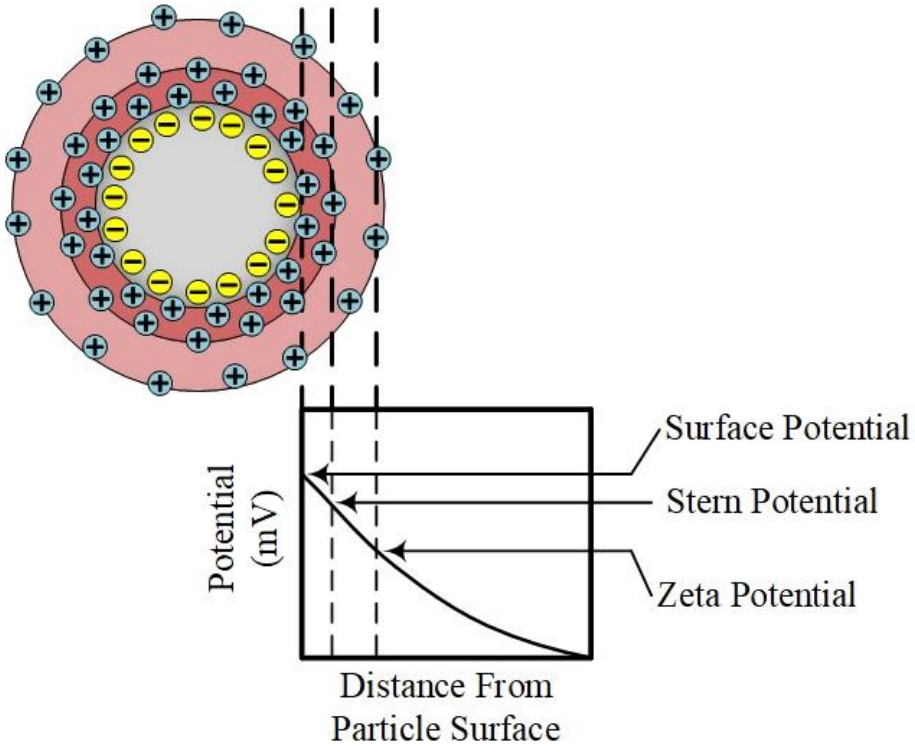

Figure 4-7 – An arbitrary particle with a negative surface charge, attracting positively charged ions or positive molecule poles.

Figure 4-8- Malvern Instruments Zetasizer cuvette front and side view. Gold-plated electrodes pictured allow for the inducing of particle motion with an applied alternating current and voltage power supply. Laser scattering occurs at the bottom.

Chapter 5 - Experimental Results

LiF Recrystallization with EC

Ethylene carbonate (EC) was reported to behave as a strong solvent (12.9 g L^{-1} at 60 ˚C [32]). 33 g, or 25 mL of EC (natural enrichment, purchased from Fisher Scientific), was heated to 90 ˚C (linearly predicted solubility of 0.6 g) in a borosilicate beaker and combined with 0.43 g LiF. 2 LiF-backfilled MSND diodes were imaged with a Hitachi S3400N scanning electron-microscope (SEM) and their masses were measured. The diodes were submersed into the EC:LiF mixture on their sides (Figure 5-4), after having been mixed.

Table 5-1 - EC solvated recrystallization of LiF in LiF-backfilled MSNDs.

Device	LiF-Filled Mass (g)	EC-Processed (90C-40C) Mass (g)	EC-Processed (80C-45C) Mass (g)	EC-Processed (50C-40C) Mass (g)	EC-Processed (93C-69C) Mass (g)
A	0.2100	0.2087	0.2083	0.2081	n/a
B	0.2080	0.2074	0.2073	n/a	0.2077

At this point, the LiF was no longer visible within the solution as a particulate. The beaker was cooled down to 40 ˚C over 30 minutes, corresponding to a change of solubility (of the 25 mL of EC) of 0.47 g LiF with a final solubility of 0.13 g LiF. Diodes were removed

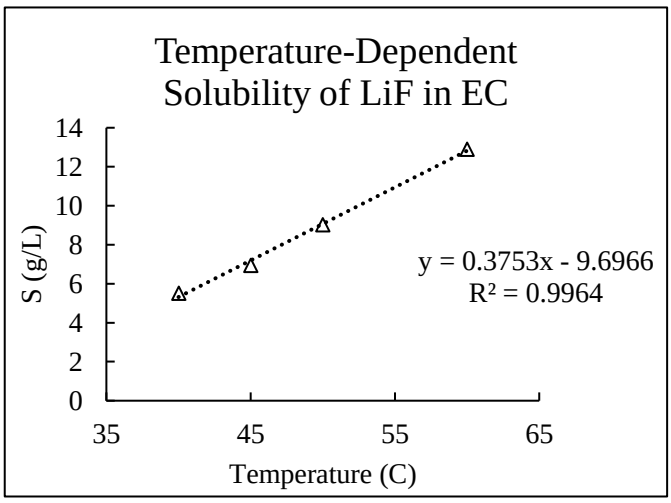

Figure 5-1 - Solubility of LiF in EC as reported [33]

from the beaker, gently placed into de-ionized (DI) water (a strong solvent of EC but not LiF) soaked for 1 minute, and then dried on hot plates. The devices were then weighed after drying. In each device, the mass of LiF was measured to decrease (Table 5-1). Observation of the experiment suggested that the cooling time of 30 minutes for a 50 ˚C temperature variation was non-ideal for recrystallization as the process may preferentially result in nucleation with the given parameters.

The experiment was reproduced with a longer cooling time to increase likelihood of recrystallization. The devices were used again in the same EC:LiF mixture with a different temperature range of 80 ˚C to 40 ˚C, which was cooled over the duration of 1 hour. In the same manner the diodes were introduced to the same solution, positioned on their sides (providing open contact between the trenches and bulk solution). After 1 hour of cooling the devices were removed, soaked in DI, dried on a hotplate, and weighed (Table 5-1). Again, the devices had slightly lower mass (albeit fractions of a milligram). To decrease the rate of cooling even further, and improve thermal control, the same solution (beaker) was placed in a water bath. Device A was placed in the solution at 51 ˚C and cooled to 40 ˚C over 1 hour. After the hour, the diode was removed, soaked in DI, dried on a hotplate, and weighed. For a third time, the device exhibited no mass gain from recrystallization (Table 5-1). Concerns that nucleation was occurring in the saturated solution in preference over coarsening of the packed diode shifted focus towards experiment cleanliness. Crystallization (or nucleation) is known to occur at “seed” locations in supersaturated solutions, which can commonly be initiated by dust or particulate contamination.

Glassware (80 ml borosilicate beaker) from the KSU SMART Lab class 1000 cleanroom was further rinsed with isopropanol and DI. The glassware was then dried with lint-free cleanroom

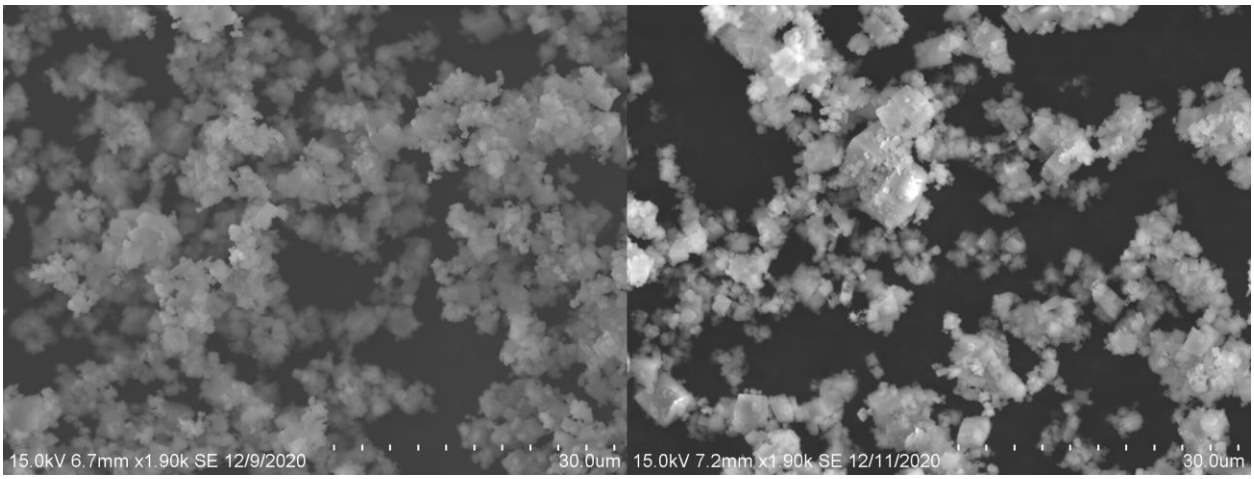

Figure 5-2. LiF before (left) and after (right) boiloff within ethylene carbonate .

wipes. 41.1 g of EC and 0.119 g of LiF were introduced to the beaker and heated directly with a hotplate to 97 ˚C (linearly predicted solubility of 0.83 g for the 31 mL of EC). Complete dissolution of the LiF was visually observed after the solution reached 97 ˚C. Diode B was introduced to the solution at 93 ˚C, and the temperature was decreased to 69 ˚C over 5 hours. After 5 hours, the device was removed, and particulate was visually observed at the bottom of the beaker. In much the same manner, the device was cleaned, dried, and weighed. For the first time a mass gain (of 0.4 mg) was measured, yet such a small measurement reasonably lay within the realm of error. Without a recrystallization of appreciable mass within the backfilled devices, the decision to attempt to nucleate LiF within the trenches of empty MSNDs was made. Empty diodes were then purposed in the used solution of 41.1 g EC to 0.119 g LiF in separate instances. A third MSND diode (A3) was wetted with DI and introduced to the solution at 101C. Steam was immediately observed, and bubbles formed within the MSND. The beaker with the MSND laid down (with trenches facing upwards) was allowed to cool down with an aluminum foil covering (to keep the solution clean). The diode was cleaned, dried, and weighed. A fourth device (D7) was dipped between 20 ˚C DI and the mixture of LiF:EC at 100 ˚C, in total 20 times. Upon final

water soaking (to remove the EC as it is miscible in water) and drying, the device showed no mass increase.

Following the unsuccessful attempt to coarsen LiF microparticles that were already packed into MSNDs, efforts were directed towards coarsening bulk particulate material. A dispersion of 100g of ethylene carbonate and 1.5 g LiF (natural enrichment) was heated within a fume hood on a hot plate until vapors were visibly observed. The production of vapors continued as the dispersion became viscous and dark brown. The solution, having evaporated EC, was anticipated to precipitate a significant mass of LiF (solubility of 20.3 g L^{-1} at 80 ˚C). The resultant brown viscous precipitate was washed with DI and the remaining particles were dried and analyzed. Resulting particulate was imaged with a SEM and particle sizes measured by Quartz PCI (image analysis software). Particles sizes, being sampled across a limited population, had not changed with any statistical significance. Additional LiF microparticles were mixed with EC in the ratio of 10g:100g of LiF:EC. The mixture was stirred with heating to 60 ˚C and left covered overnight.

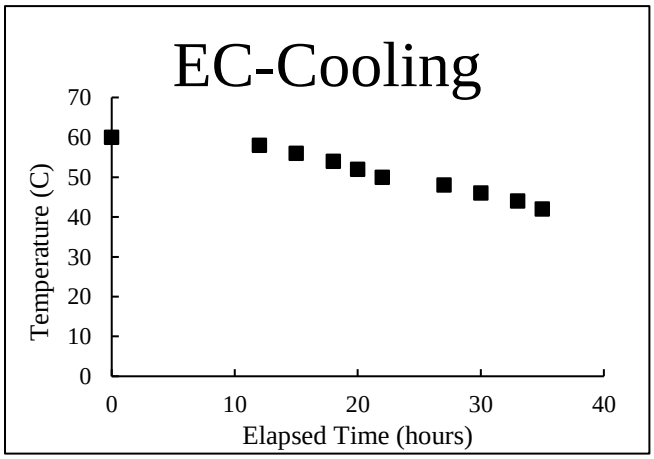

Figure 5-3 - Thermal ramp-down of EC, supersaturated with LiF. Slow cooling proceeded in an effort to drive particle coarsening phenomenon in preference to nucleation.

Figure 5-4 - LiF-backfilled MSND upright in a beaker with heated EC:LiF mixture. Diode trenches are exposed to the solution and the temperature drop is measured.

The temperature ramp-down process followed the stepwise procedure as depicted in Figure 5-3. The solubilities of LiF within EC and DMSO were tested by heating (with stirring) EC on a hot plate for over 20 hours, covered. Although LiF was reported to have solubility in EC [32] and DMSO, the dissolution of LiF within these solvents was never observed. Particle sizes never increased, an indication that material never solvated and/or precipitated out of the solution. More aggressive heating of LiF and EC revealed that LiF catalyzes polymerization of EC into an unidentified viscous brown fluid. A parallel investigation to purpose the thermal dependence in solubility with DMSO concluded without any indication of particle coarsening, a property regularly observed from supersaturated solutions. Furthermore, the similar index of refraction and white/translucent color (1.41 for EC and 1.39 for LiF) provoke the visual observation of dissolution between LiF and EC.

Metallic Lithium Backfill

Metallic lithium was handled within an inert glovebox, purged for over 12 hours with argon (and then operated with a constant flow of high-purity argon). The lithium was cleaned with p-xylenes, a non-oxygenated solvent known to not interact with lithium while degreasing mineral oil, and cleaved with a spatula. The cleaved face maintained lustrousness for over 3 minutes, indicating small quantities of moisture remained within the glovebox. During this time an MSND, empty and coated with parylene, was heated on a hot plate to >185 ˚C (the melting point of metallic lithium). The MSND temperature was measured with laser infrared thermometer and confirmed that the MSND had reached the appropriate temperature to melt metallic lithium. A fresh piece of lithium was prepared by cleaving new facets on sample, and the piece was placed onto the MSND.

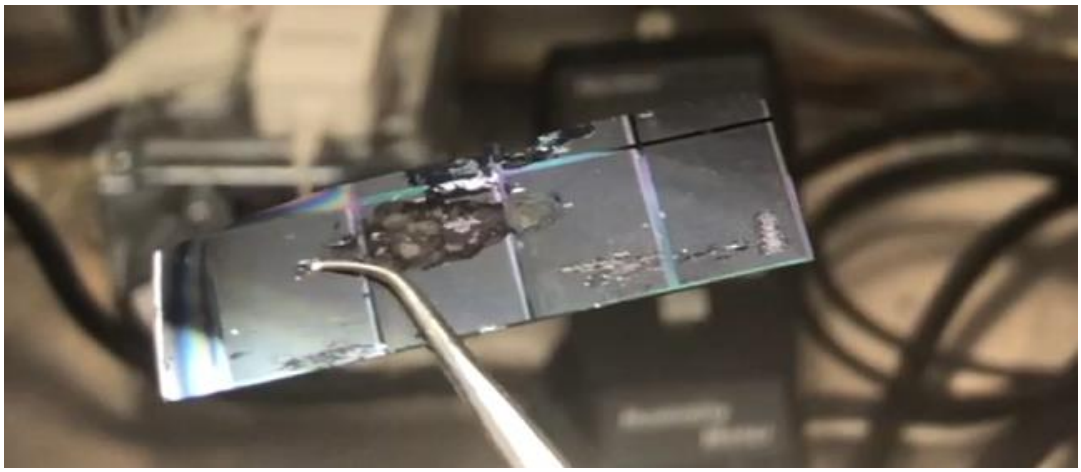

Figure 5-5 - Bare MSND upon destruction from reacting with molten Lithium, within an inert glovebox.

Immediately following the melting of lithium, a reaction between the parylene and molten alkali occurred, shredding through the fins of the microstructured device and fracturing the wafer. Crystalline grey granules appeared as a result of this reaction, expanding in total volume. This effect was replicated again, occurring immediately upon the introduction of molten lithium to the high surface area microfeatures. Afterwards, it was noted that the specific parylene variant used on the device contained fluorine (Para-F). The glovebox was prepared again for experimentation, in the same argon-purging procedures outlined before, and a bare MSND wafer was heated on a

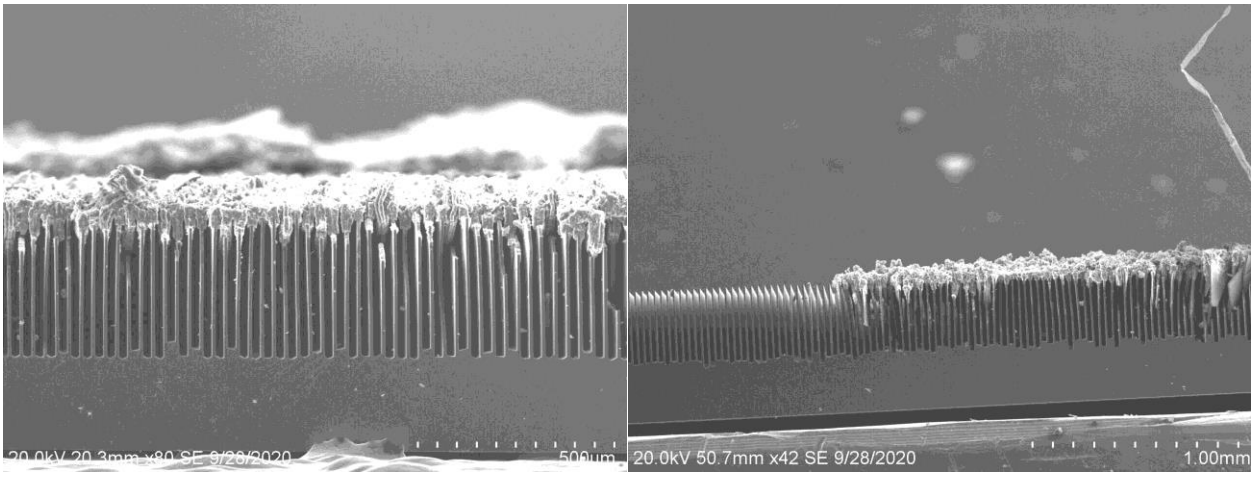

Figure 5-6 - ^{6}Li foil hand-pressed into empty MSNDs at 140 ˚C on a hot plate with stainless steel roller.

hotplate to 200 ˚C. The microfeatures, again, were destroyed upon reacting with the molten lithium (producing crystalline granules, grey in appearance). From this point, there was a concern about the chemical reaction between molten lithium and silicon. This reaction results in the expansion of silicon, which produces the apparent shredding of the silicon MSNDs. Consideration was provided to lithium-passivation coatings (to prevent reactions between the substrate and lithium), that are capable of withstanding the temperature of 185 ˚C. The passivation coatings, if exposed to high-temperature lithium, should be devoid of oxygen and halides. The primary passivation coating considered in this matter was parylene (without halides).

Figure 5-7 - A Parylene-N coated wafer, sandwiched between parchment paper (cellulose), which was pressed with a manual roller above 200 ˚C on a hot plate. Lithium was successfully melted without violent reactions.

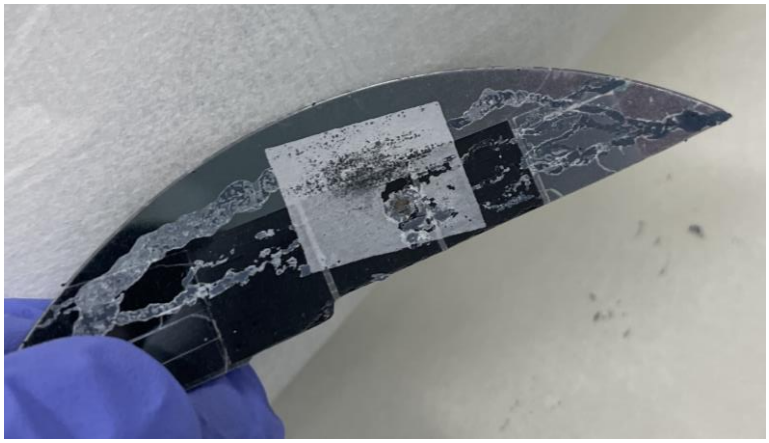

Figure 5-8 - A Parylene-N coated wafer (Figure 5-7), upon uncovering revealed visual damage to the underlying MSNDs.

Investigation into the plastic deformation of heated lithium foils yielded poor results with only superficial deposition. Empty MSND wafers were then coated in both Par-N and ParyFree® (non-

halogenated proprietary parylene coating) by a third party vendor and subjected to heated pressing of lithium foil.

Wafers were introduced into a dry room (<0.1% RH and < -50 ˚C dew point) and acclimated for 24 hours. A heated laminator (Apache A18) was preset to 140 ˚C and allowed to warm up for 30 m. A segment of 55 µm-thick ^{6}Li foil was folded on top of the wafer (trenched side) and the experiment was "sandwiched" between 2 segments of PTFE sheets (~1mm thick). The materials were then passed through the laminator 4 times with 90-degree rotation between passes; after uncovering the wafer and foil, it was realized that no plastic deformation was occurring within the operating temperature and pressure. The laminator temperature was increased to 180 ˚C, and the experiment was repeated. Still no plastic deformation with resulting lithium backfilling the trenches was observed. Processing the wafer and foil with PTFE sheets at a temperature of 200 ˚C yielded a fluorine-leaching reaction between the PTFE and metallic lithium, with visible black "burn" marks appearing on the polymer sheets.

Further investigations into metallic lithium backfills purposed cellulose sheets (parchment paper) as a passivated layer between rollers (laminator and manual rollers) in an attempt to work with metallic lithium at even higher temperatures. Laminator pressures were again too low to produce anything beyond superficial backfill of metallic lithium, which was observed as metallic lithium "sticking" to the tops of

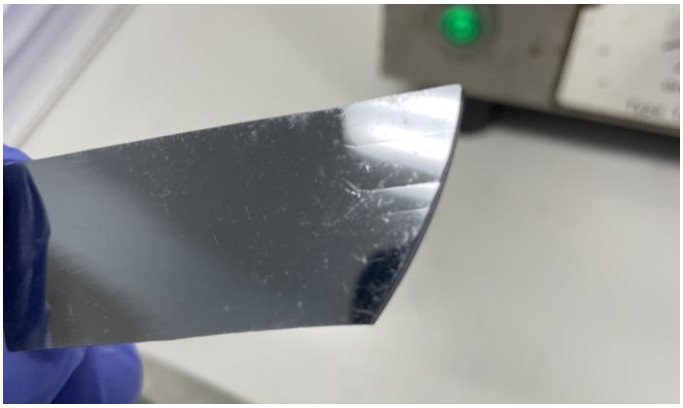

Figure 5-9 - The backside of an empty MSND wafer segment, coated in Parylene-N, fracturing from thermal stresses in the polymeric film.

the fins. Hand-rolling with a silicone brayer (parchment paper between lithium and roller) on Par-N demonstrated poor thermo-mechanical behavior and continuously destroyed empty MSND wafers as a result of thermal contraction; this was observed during heating while lacking any lithium on a hot plate. ParyFree, when heated, exhibited no thermal-induced destruction of the wafers. The ParyFree polymer appeared to not react with molten lithium, either. The ability to fill the trenches with molten lithium was unsuccessful, and no plastic deformation of heated lithium foil into the trenches was observed. The metallic lithium experiments were unsuccessful and ultimately abandoned.

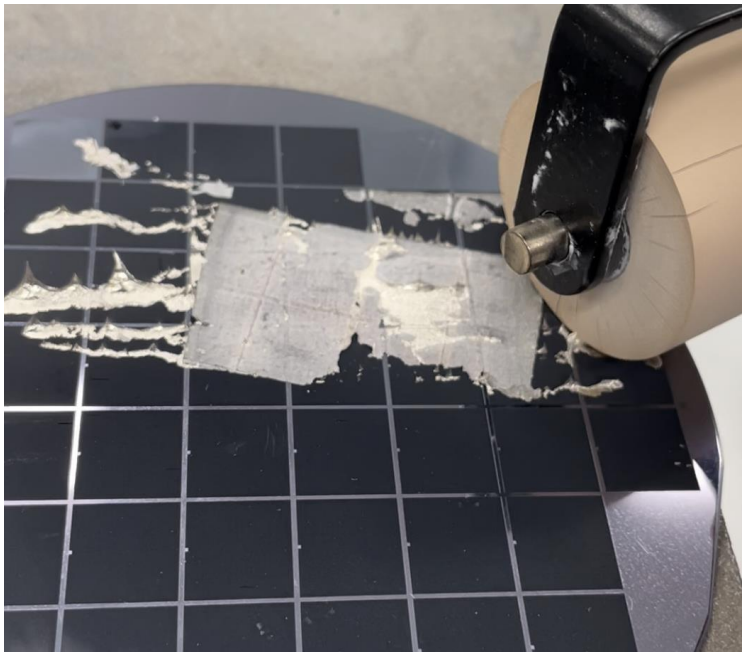

Figure 5-10 - ParyFree coated MSND wafer, with molten lithium being pressed against the trenches by a silicone manual roller.

Particle Size Measurements and Control

Particle size measurements were conducted with a green laser (532 nm), measuring the light scattered at 90 degrees with a photomultiplier tube; the tube output was then coupled to an ALV (multiple tau) digital correlator, which interfaced with a PC and the associated ALV software for autocorrelation and eventual particle size measurements. Microparticulate ^{6}LiF from RDT MSND production stockpiles was analyzed in a dispersion of dimethyl formamide (DMF), a common DLS dispersant in the facility that was used with no known solvation properties of LiF.

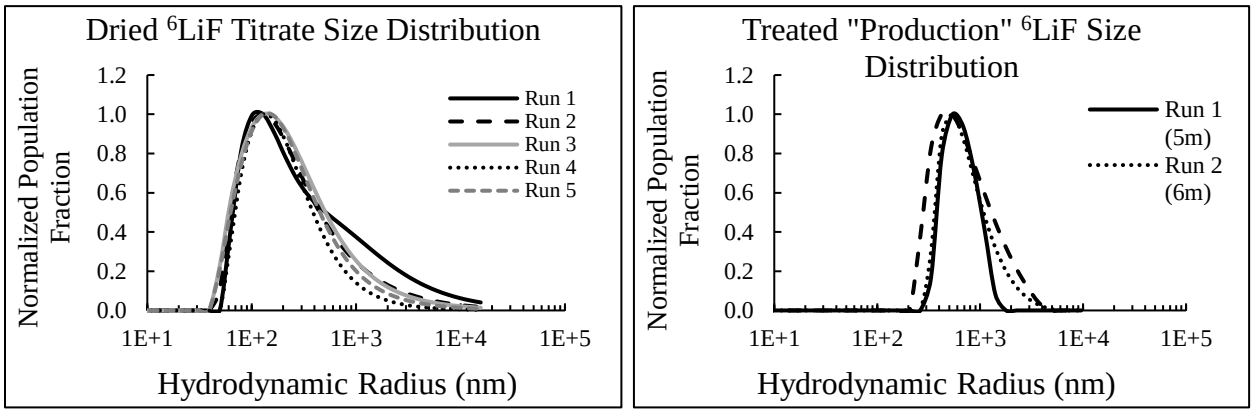

Figure 5-12 - Dynamic Light Scattering Measurements, Sampling Particle Size Distributions After 5 Minutes of Settling of Microparticulate ^{6}LiF. At this point, it was certain that particle ripening was negligent and the nomenclature "washed/treated" was purposed to denote production-ready material.

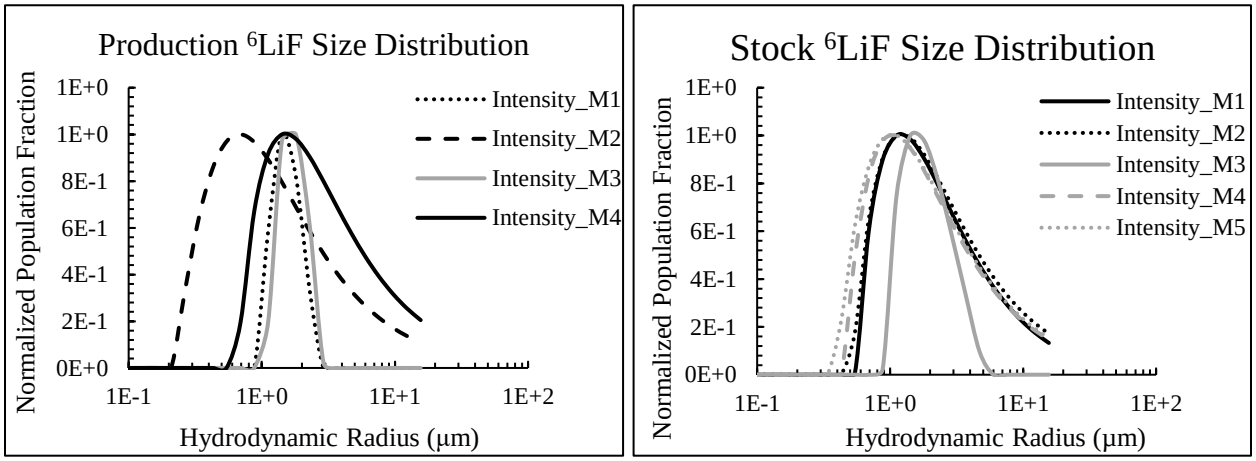

Figure 5-11 - Particle size distributions following agitation by pipette within a quartz cuvette, for the first 4-5 minutes after agitation. RDT MSND production ^{6}LiF (thought to be ripened) is measured on the left and purchased LiF measured on the right.

The yielded particle size distributions indicated high polydispersity, which was expected when considering the micrographs of the same material depicted a wide variety of particle sizes (Figure 5-13). The measurements taken from the dispersion of the production ^{6}LiF were, however, unrepeatable; allowing the dispersion to settle for 1-minute resulted in particle size distributions that were remarkably different (Figure 5-11). The apparent instability in the dispersion yielded particle size measurements that were not reproducible or acceptable for the microparticulate. The nanoparticle distributions, however, won't suffer from this effect due to their longer settling times;

a consistent settling period could be purposed to sample the nanoparticle size distributions from the "ripened" ^{6}LiF for comparison to the control ^{6}LiF. From this method, measurements (Figure 5-12) indicated that particle ripening cycles reduced the population of nanoparticulate ^{6}LiF, an intuitive finding when considering particle ripening mechanics. Once values were experimentally obtained for the diffusion coefficient of ^{6}LiF (by DLS) and the interfacial energy was determined (570 erg cm^{2}), a kinetics model was formed for the ripening of ^{6}LiF in H_2O (Figure 5-14, and Eq. 14). The model, called "LSW Theory" (named after the scientists Lifshitz, Slyozov, and Wagner) relates the quantities and properties: This model indicated that the ripening of microparticulate LiF would be presumably negligible within the timeframe of less than 100 hours. It was determined that the particle "ripening" (herein referred to as "washing") cycles were not coarsening microparticulate as much as previously thought, and only nanoparticules would experience a (relatively) significant coarsening. This finding eluded that a different effect was occuring during particle washing cycles that improved the ability to pack the microparticulate into the MSNDs.

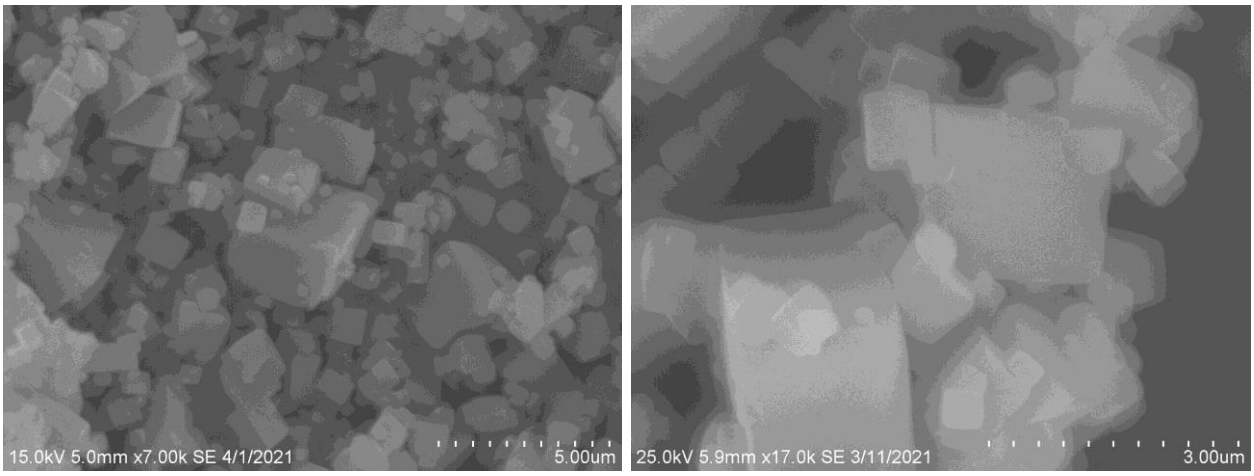

Figure 5-13 - Polydisperse micro/nano-particulate ^{6}LiF, sampled from RDT MSND production stockpiles. ^{6}LiF particles were sputtered with 20 nm gold to improve micrographs.

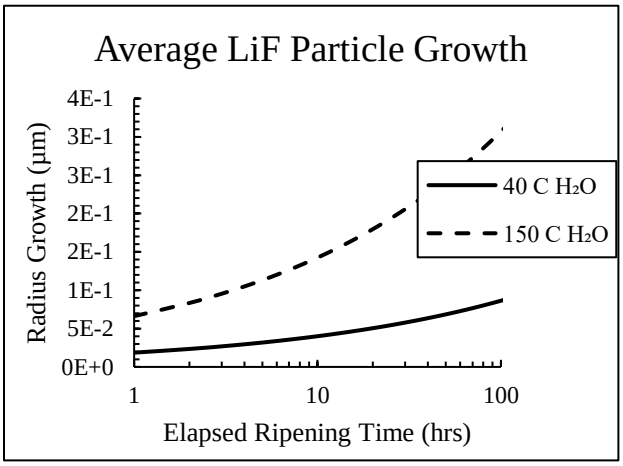

Figure 5-14 - LSW (from Lifshitz, Slyozov, and Wagner) ripening kinetics of LiF in H_2O, with the diffusion coefficient sampled from DLS and surface energy of 570 erg cm^2 [47].

The kinetics of precipitation from supersaturated solid solutions [34]

$$R^3 - R_0^3 = \frac{8\gamma c_\infty V^2 D}{9 R_g T}\, t\,, \qquad (14)$$

R: Particle Radius (t)
R_0: Initial Particle Radius
γ: Interfacial Surface Energy
c_∞: Solubility in Solution
v^2: Molar Volume
D: Diffusion Coefficient
R_g: Rydberg Gas Constant
T: Temperature
t: Time

While trying to control particle sizes to improve particle packing, a top-down approach was explored. This top-down method sought to produce large crystals of ^{6}LiF by smelting and then grinding the large crystals into microparticles of sizes not achieved by particle coarsening attempts. Previously cast ^{6}LiF (cast in open atmosphere) fragmented into smaller pieces by a hammer (~1 cm diameter for the largest pieces) and then were ground in an industrial grinder for

150 seconds. The resultant material produced a pungent sulfuric smell upon the opening of the grinder and appeared as a bulk white particulate. The ground particles were imaged with SEM and were visually more polydisperse than the cubic microparticulate previously shown. The particles were remarkably more irregular in shape, a result from grinding that would affect the

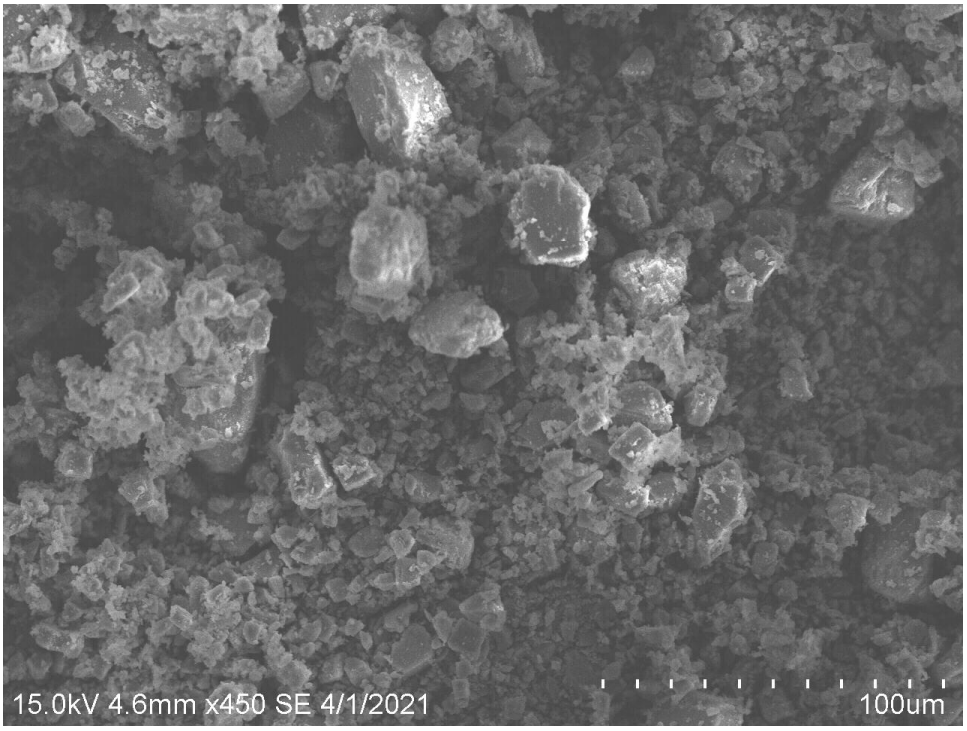

Figure 5-15 - ^{6}LiF particulate ground for 150 seconds from open-air castings

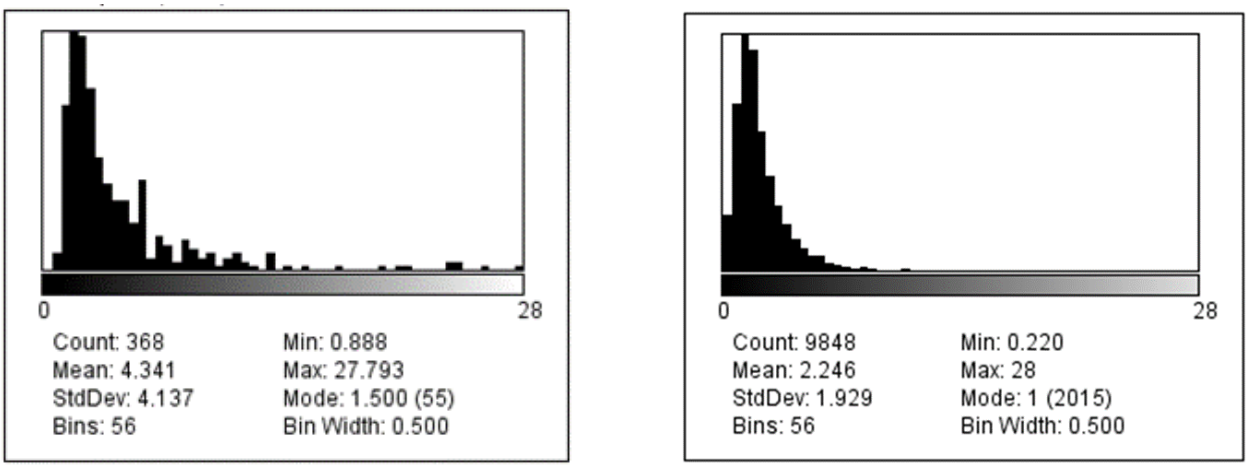

Figure 5-16 - Manually measured ground ^{6}LiF (left) from 4-1-21, and automated image-analysis measurements (right) from the same micrograph, both in units of µm.

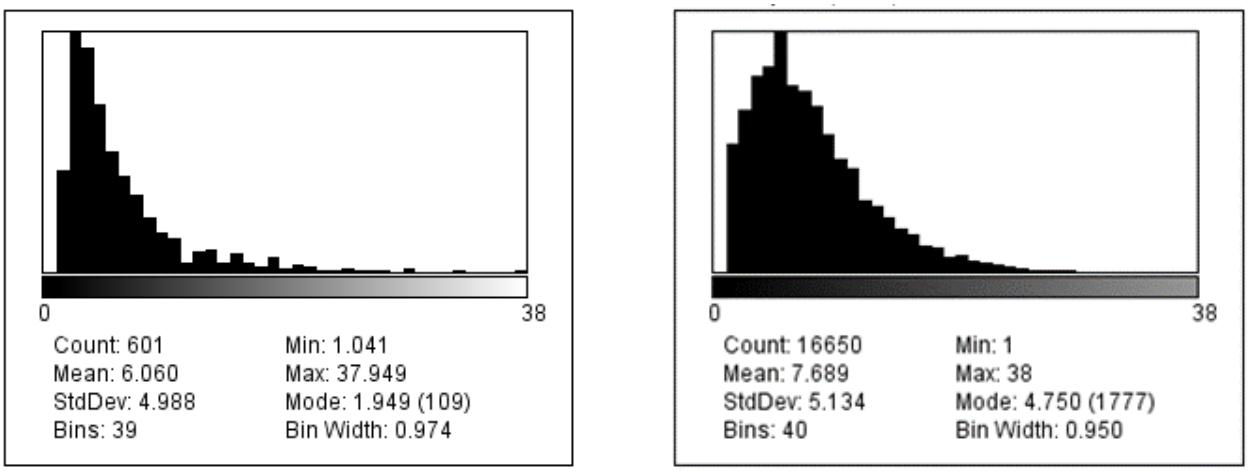

Figure 5-17 - Manually measured ground ^{6}LiF (left) from 5-28-21, and automated image-analysis measurements (right) from the same micrograph, both in units of µm.

ability to achieve close packing. The material appeared larger in mean particle size, and thus unlikely to be measured adequately with DLS; furthermore, the measurement of particles manually with micrographs was a task vulnerable to human bias/error and poorly scalable. For the reasons aforementioned, an automated visual particle analysis methodology was considered.

Visual particle sizing using image processing algorithms and micrographs is commonly used for materials which don't form stable aerosols or dispersions (or exhibit poor light scattering behavior). ImageJ was purposed to perform image modification: contrast enhancement, blur, morphological filter [35], morphological segmentation [35], watershed line production, erosion, and subsequent measurement. Using the min-feret measurement, the highly irregular particle shapes were measured in the smallest visible dimension that controlled their ability to pack into the MSND trenches. A comparison was made from manual particle measurements and automated measurements from ImageJ. Results from manual and automatic measurements varied by as high as 2.2µm in min-feret diameter (Figure 5-16, and Figure 5-17) and were affected by particles stacking atop another when imaged. Loose packing (without significant compression) of particles

is known to achieve packing fraction maxima for larger particle diameters [36], without consideration to the maximum allowable particle size encountered for HAR microstructures.

Zeta Potential, Surfactants, and Particle Treatments

The behavior of particle agglomeration was experimentally investigated to produce dispersions capable of propagating particulate LiF into the MSND trenches. Prior expertise with particle packing inferred that packing challenges would be likely dictated by the interactions between particles [36]. Such interactions are commonly manipulated by the addition of surfactants to dispersions, yielding stable dispersions or halting agglomeration. Previous work examined the use of hydrogen peroxide and acetic acid to reduce the agglomeration of microparticulate LiF [5], with acetic acid being a documented surfactant of LiF [37]. Microparticulate LiF was noticed to pack MSNDs poorly as a result of usage, requiring a particle "washing" after each use to achieve the 30-40% packing fraction manufacturer standard.

Measuring the ability to pack LiF under the influence of different surfactants is not trivial, provided a large supply of LiF and empty MSND wafers; unfortunately, manufacturer's specification empty MSND wafers are a costly resource. A secondary technique to measure the ability of particle packing was needed, purposing quantifiable particle behavior instead experimental packing results in empty MSND wafers. To characterize particle packing behavior, zetapotential measurements were taken for some selected particle treatment materials (Figure 5-18). LiOH was investigated as a particle treatment material upon the discovery that ^{6}LiF became basic throughout the particle washing cycles. O_2 plasma (from a cleanroom asher oven) was

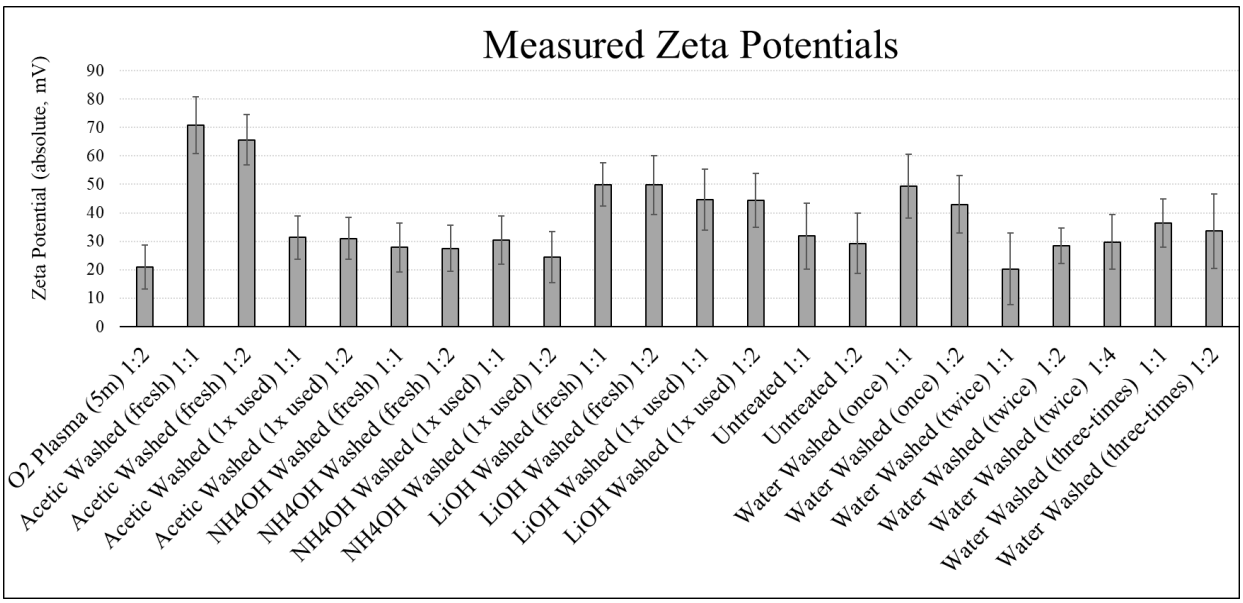

Figure 5-18 – Zeta potentials measured for ^{6}LiF with various particle treatments, using a Malvern Zetasizer Nano ZSP. Ratios at the end of the labels denote a decrease in dispersion concentration to test samples for multiple-scattering influence. Values are displayed as absolute but were all measured negative.

explored as an option to oxidize lithium fluoride (forming LiO) on particulate surfaces, which yielded a remarkably low zeta potential.

Particle washing proceeded in a similar manner for all materials: a combination of the treatment material (acetic acid, LiOH, etc) and ^{6}LiF were mixed with DI and heated to 160 ˚C overnight (between 16-20 hours). The resultant material was stored in sealed individual labeled polymer tubes for future analysis. Because ^{6}LiF packing is performed in methanol, Zetapotential dispersions purposed methanol as a dispersant with ratios of 45mg:10mL of "washed" ^{6}LiF and methanol. Methanol, a hydroscopic alcohol is known to absorb moisture from the air, and all measurements were preformed without preparation of dispersions within a dry glovebox. The influence of moisture on zeta potential measurements has previously been investigated for ZnO nanoparticles within methanol dispersions, indicating that the presence of moisture increases the

variance of observed zeta potentials up to 8 mV for water concentrations between 20 – 375 $\mu L_{H2O}/L_{Methanol}$ [38]. Such dry preparations should be exercised in future studies of the zeta potentials of treated microparticulate ^{6}LiF. Methanol is also known to undergo electrolysis at voltages as low as 0.03 V [39], for which the gases hydrogen and carbon dioxide would evolve at the anode and cathode, respectively. If such gases were to evolve and adsorb to the surfaces of the particulate dispersions, it is suspected that hydrogen reduce upon negative ionic surfactants resulting in a decreased absolute zeta potential, which was not observed during measurement.

Confirmation of ^{6}LiOH as a particle-packing enhancer (surfactant) was made through experimental packing of empty MSND wafers. ^{6}LiOH, acetic acid, and ammonium hydroxide-treated particulate were all used to backfill MSNDs in the same manner as manufactured commercial devices (as was an untreated control). Dispersion of methanol and treated ^{6}LiF particulate were blended and poured atop face-up empty MSND wafers, which were cushioned from below with silicone pads, within 1500 mL borosilicate beakers. Wafers were weighed and leakage currents measured at -3V (reverse bias) in a dark-box probe station beforehand. The beakers were then loaded into a Quantrex Q650H ultrasonicator bath and sonicated for 1 hour. The devices were removed, dried, cleaned, weighed, and leakage currents measured (Figure 5-19). The packing fractions were calculated for nominal trench parameters of 400 µm depth and 20 µm width (Table 5-3). Acetic and ^{6}LiOH - treated material was then packed into empty MSNDs with mechanical pressure applied after sonication (while still wet, by a manual roller). The packing fractions increased significantly and reproduced upper yields on packing for production (H_2O-washed) material. Acetic acid, in adjacent backfills, resulted in significant (>10%) increase in diode failure due to leakage current increase.

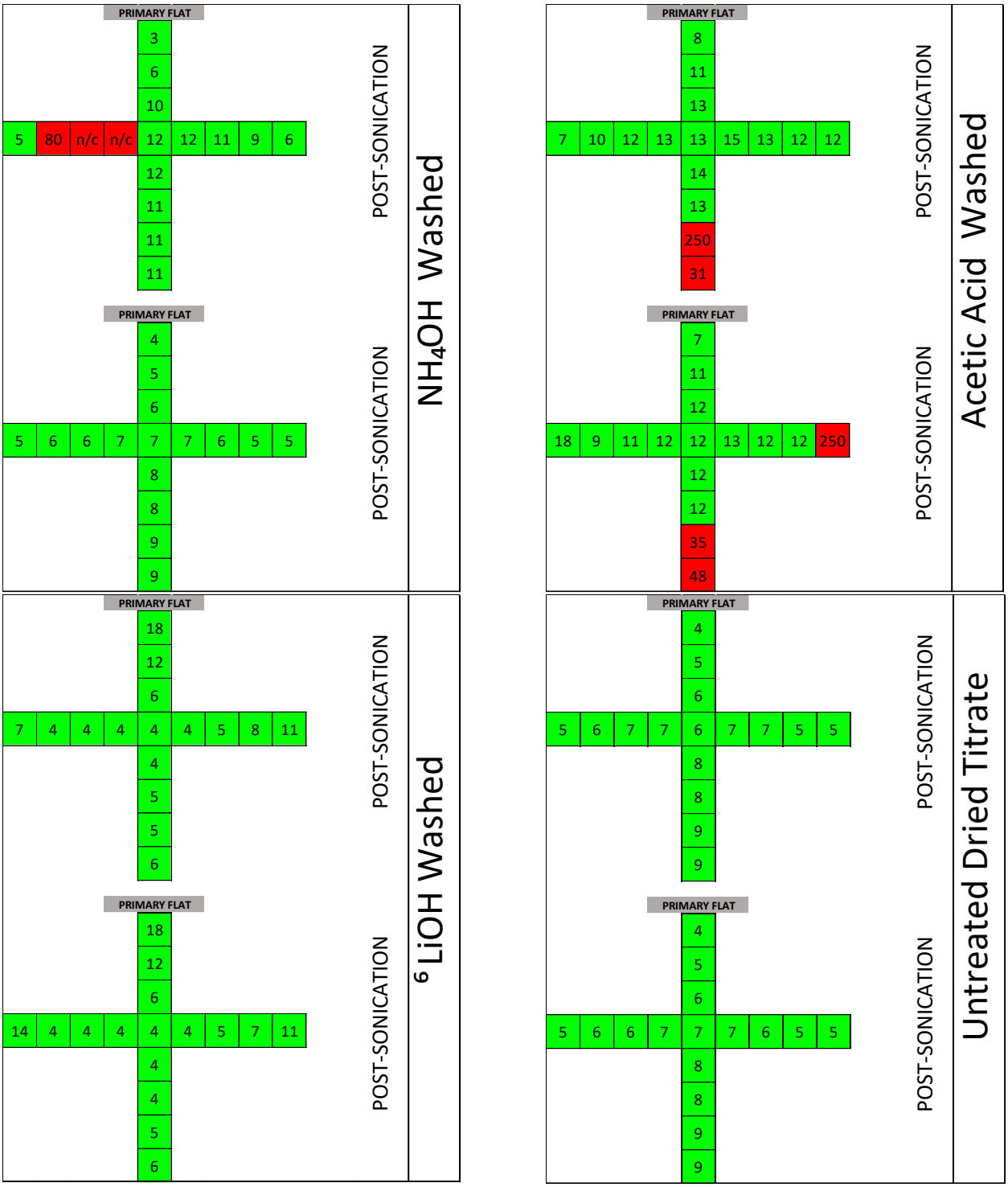

Figure 5-19 - Leakage currents measured in -3V (reverse bias) for selected diodes on each wafer. Each wafer was processed in a mixture of 0.33L methanol to 10g of treated material for 1-hour of sonication. Note the Ammonium hydroxide-washed wafer reflects 3 diodes that passed leakage current tests (<25nA in reverse bias, with >100µA in forward bias) after processing, a result of cleaning the bonding pads. Devices not achieving >100µA in forward bias are denoted "n/c", indicating poor electrical connection between the electrical probe and the diode, through the bond pad.

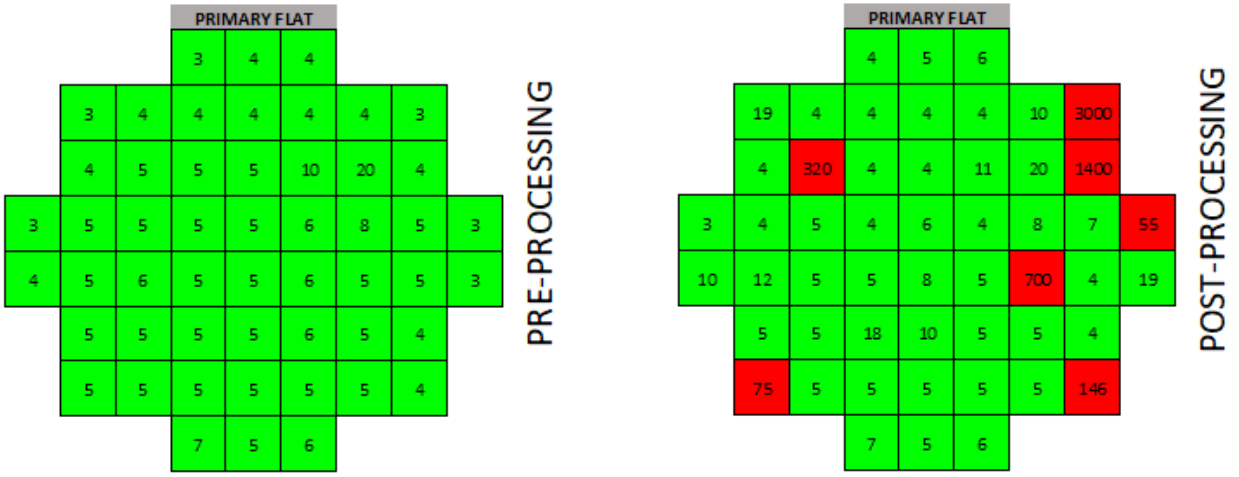

Figure 5-21 – Leakage current measurements in -3V (reverse bias) for empty MSND wafer backfilled with ^{6}LiOH-treated ^{6}LiF. Wafers were sonicated for 1h with 333 mL methanol to 10g treated ^{6}LiF. Following sonication, the wafers were dried, weighed, and then packed by hand with methanol-wetted treated ^{6}LiF, using silicone brayers.

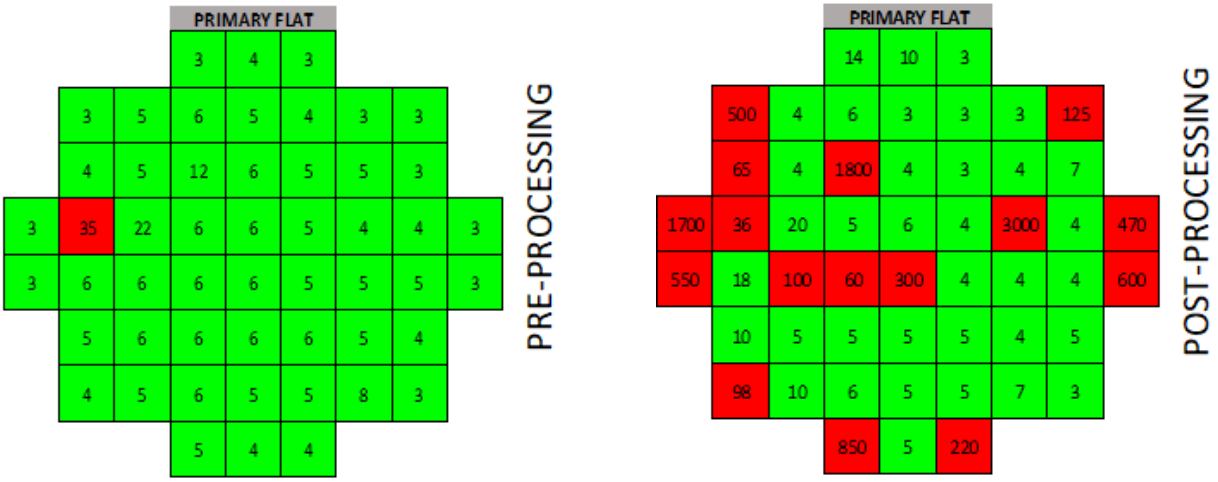

Figure 5-20 - Leakage current measurements in -3V (reverse bias) for empty MSND wafer backfilled with acetic acid-treated ^{6}LiF. Wafers were sonicated for 1h with 333 mL methanol to 10g treated ^{6}LiF. Following sonication, the wafers were dried, weighed, and then packed by hand with methanol-wetted treated ^{6}LiF, using silicone brayers.

Previously, methods coupling sonicated tamping with weights purposed glass beads to help backfill MSNDs. These beads, while producing no visually observable damage to the diodes, destroyed the diodes yielding MSNDs with unacceptably high leakage currents in reverse bias. This method was further investigated with plastic weights, cut from a 1" thick sheet of HDPE. The weights were small enough in diameter to fit into 1400 mL borosilicate flasks and overlap the

entire 4” of diameter of the empty MSND wafers. The weights each weighed approximately 220 grams (with the galvanized screw handles included). A slurry of the material from the “top-down” process was mixed with methanol in a ratio of 30g:10mL. The beaker was loaded with an empty MSND wafer (weighed prior), which the slurry was poured atop. The slurry, appearing thin, was thickened upon the addition of dry LiF powder by hand. The wafer, with thickened slurry on top, was covered with a single 220 g HDPE weight and methanol was added until the weight was just covered. The beaker was placed into a sonic bath and sonicated for 2 hours, covered with Parafilm.

After 2 hours, the sonicator turned off and the beaker was allowed to sit overnight. Upon drying the next day, the wafer was weighed, reheated, and weighed again. From the measured weight and trench characteristics (once cleaved and imaged in a SEM), the wafer was concluded to have a packing fraction of 54 ± 4.2%. This result was replicated again in the same manner with a mechanical (undoped) wafer, resulting in a packing fraction of 46%. After yielding such high packing fractions, a third wafer (doped) was purposed to determine if the process was damaging the diodes by measure of leakage current in reverse bias. The third wafer produced a 51 ± 7% packing fraction while introducing less than 4% loss of diodes due to leakage current increase.

The weighted-sonication method was purposed at a larger scale, processing 6 wafers simultaneously within the same bath (Figure 5-23), similar to the method in which MSNDs are currently backfilled. This first VLSI production run using the weighted-sonicated technique yielded undesirable results (Figure 5-26). Packing fractions varied heavily with a range of 30-49% (trench measurements of 400 μm depth and 20 μm width). After the first six wafers were

backfilled, adjustments to the slurry were made (20g:7mL). Two wafers were sonicated within the Quantrex 650H at the same time, using the top-left and bottom-right "slots".

Table 5-3 - Packing fractions for the highest-performing treated particulate, with manual packing.

Acetic Acid Washed	LiOH Washed
44%	39%

Table 5-3 - Packing results for treated ^{6}LiF without manual packing.

	Untreated Dried Titrate	Acetic Acid Washed	NH_4OH Washed	^{6}LiOH Washed
PF	18%	15%	18%	20%
dM (g)	0.64	0.54	0.62	0.70

A second VLSI attempt at weighted-sonication backfill was made with the new ratio of 20g:7mL (^{6}LiF:methanol) and 6 wafers were backfilled simultaneously, with a 2nd sonication duration of 2 hours (4hrs total sonication, instead of 3 hours). Again, the results showed that many wafers sonicated at once in the Q650H sonicator was undesirable. Concerns about the sonicator transducers arose and the method was adapted for a single-wafer system in a smaller sonicator. A

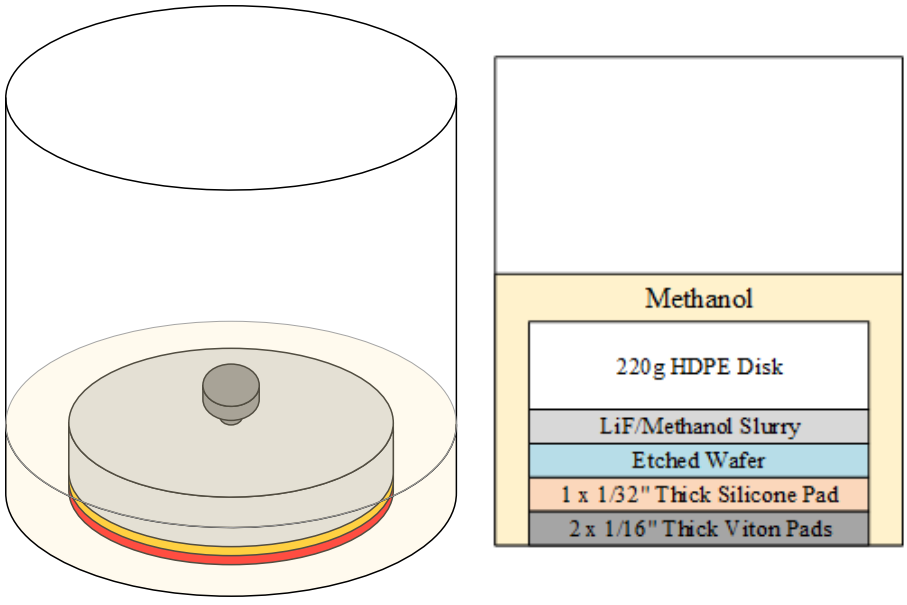

Figure 5-22 - Layout of a 1500 mL borosilicate beaker prepared to perform the weighted-sonicated method of backfill.

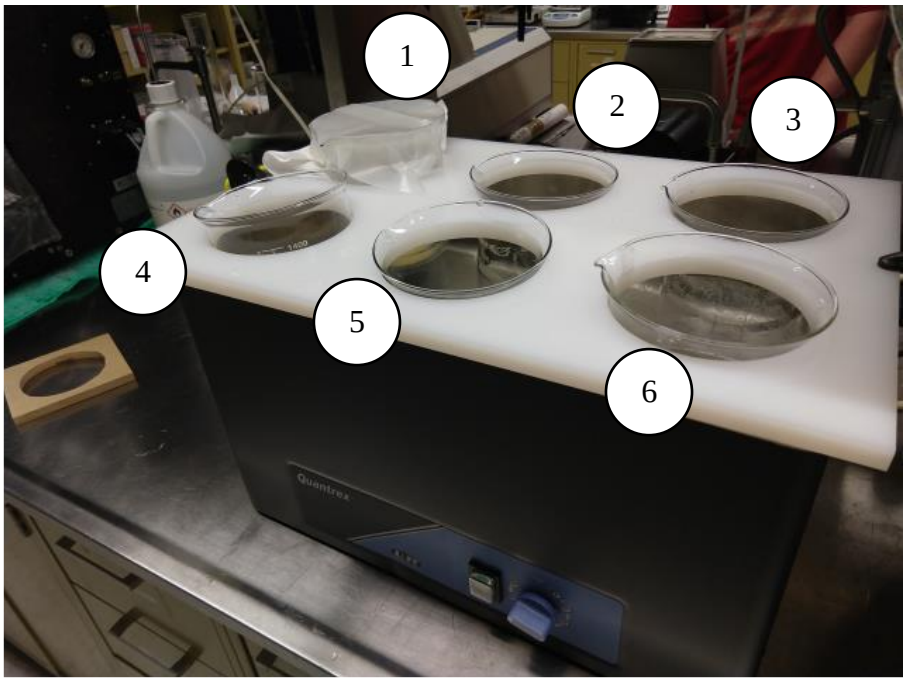

Figure 5-23 - A Quantrex 650H sonicator with polymer sheet cut to hold 6x 1500 mL beakers in suspension within the sonicated water bath [5]. Positions are referenced 1-6, as their locational effects were determined to alter the outcome of backfills.

Fisher Scientific FS20H sonicator was used with a single wafer and achieved a 39% packing fraction. An additional single-beaker sonicator was purchased in a 200W model and tested. Initial results yielded packing fractions of 48% and 39%, well within the uppermost yields of commercial devices. After further experimentation, the packing fractions fell to below 30% consistently.

The method was ultimately abandoned as the reproducibility dwindled. Backfills seemingly depended entirely upon the particle size distribution which dictated the slurry viscosity. Slurries would thicken too much upon sonication, which produced heat resulting in solvent evaporation, or thin slurries would flow out from underneath the weights leaving the interface between weights and wafers lacking ^{6}LiF to backfill. Packing performance decrease due to use of the material was not initially notice, but later observed. The casting of ^{6}LiF for the "top-down"

material is thought to have produced $^{6}LiOH$. The influences of sonicator power and backpad dampening were observed without thorough characterization, and the standing waves within the system were characterized. A more thorough approach to this methodology is suggested to include characterization of the sonic waves experienced within the beakers, quantification of the sonic power introduced into the beaker, and optomization of these parameters for backfills.

43%	38%	34%
30%	30%	49%

Figure 5-26 - Packing fractions for first VLSI run with weighted-sonicated backfill. Locations in this diagram reference the overhead locations in the sonicator.

35%	27%	30%
30%	20%	26%

Figure 5-24 - Packing fractions for the 2nd VLSI trial. Locations in this diagram reference the overhead locations in the sonicator.

42%		
		43%

Figure 5-25 - Packing fractions for the last 2 wafers of the first VLSI run. Locations in this diagram reference the overhead locations in the sonicator.

Li_2O_2 was recrystallized within the trenches of empty single-die MSNDs with limited success. A supersaturated solution of 0.5M Li_2O_2 (with DI) recrystallized within the devices, yielding mass depositions as high as 14 mg, which resulted in estimated Li_2O_2 packing fractions as high as 20%. When examined, the diodes revealed dendritic growths at the tops of the trenches that prevented the penetration of a supersaturated solution into the trenches of the diodes. The

experiment was repeated, utilizing covered petri dishes to reduce the rate of evaporation (and resultant recrystallization) in an effort to preferentially recrystallize instead of nucleate.

The devices were treated with the supersaturated solution by dropwise addition to the top surface, maintaining the solution on the top by surface tension. The diode trenches became visibly wetted during this process, and the recrystallization of Li_2O_2 was noticed to occur preferentially along the surface of the solvent (sitting on the top of the diode). Diodes were weighed and showed less mass gain than the uncovered experiment. Li_2O_2 was noticed to recrystallize rapidly from supersaturated solutions, form dendritic crystalline structures (Figure 5-27), and effectively yield low packing results (from the process of recrystallization). Additionally, the material is known to react with the moisture in air, producing LiOH, a reaction that would expand the apparent backfill posing a hazard to the fragile microstructures. The formation of LiOH was, however, hypothesized to be minimal after analysis of the diodes upon soaking in a beaker of methanol (50 mL, with solvation up to 70 mg LiOH). Energy-dispersive X-ray Spectroscopy (EDS) of the cleaved sample before and after soaking failed to indicate significant presence of carbon from lithium carbonate, an additional product of Li_2O_2 reacting (with carbon dioxide).

Measurements of the mass-loss as a result of methanol soaking for a single diode resulted in a 7% mass loss, indicating that the procedures could still yield backfills of Li_2O_2 of 15% for empty diode if 7% of the apparent mass was from LiOH. A diode, previously filled with microparticulate ^{6}LiF (unknown packing fraction) was capable of recrystallizing 7 mg of Li_2O_2, corresponding to an estimated packing fraction of 8%. The capability to enhance a backfill of LiF by recrystallization of Li_2O_2 with an 8% packing fraction of Li_2O_2 is a notable feature of this

material, as the packing fractions corresponding to maximum efficiency with LiF are regularly unattainable with standard sonicated (and manual rolled) mechanical backfill methods. An 8% increase in packing fraction for a MSND can yield an estimated 3% efficiency increase for MSNDs with a 40% packing fraction (as both backfills behave similarly in simulated efficiencies, Figure 5-28).

The ΣL product was shown to maintain an accurate parameter in determining the ability of a material to convert neutrons to maintain low energy-transfer between conversion-products and the converter. ^{6}LiF maintained the highest performance among stable materials at 60% efficiency for a simulated LLD of 300 keV and 40% for an LLD of 1.6MeV (the recommended LLD for high gamma rejection by RDT). At these values, corresponding to approximately 60% packing fraction for MSNDs, metallic ^{6}Li begins to overcome all candidate backfills in performance. While the atomic density of ^{6}Li is lower in metallic lithium, the high ion transmissivity lends to minimal energy loss of the conversion products within the backfill material and maximum energy transfer to the semiconductor. Conversely, the heavier alkyl halides (^{6}LiI, ^{6}LiBr, and ^{6}LiCl) produce the lowest performing backfills as the conversion products interact much more with the charge-dense material and do not counter this effect by the high-atomic density of ^{6}Li, as in the case of ^{6}LiF. All plots indicate that the highest efficiencies for these geometries, LLDs, and materials would lie with $^{6}Li_3N$ and metallic ^{6}Li. Considering the chemical reactivities of Li_3N, Li_2O_2, and metallic lithium, the best candidate backfill for ^{6}Li-based MSNDs (and variants) is conclusively ^{6}LiF.

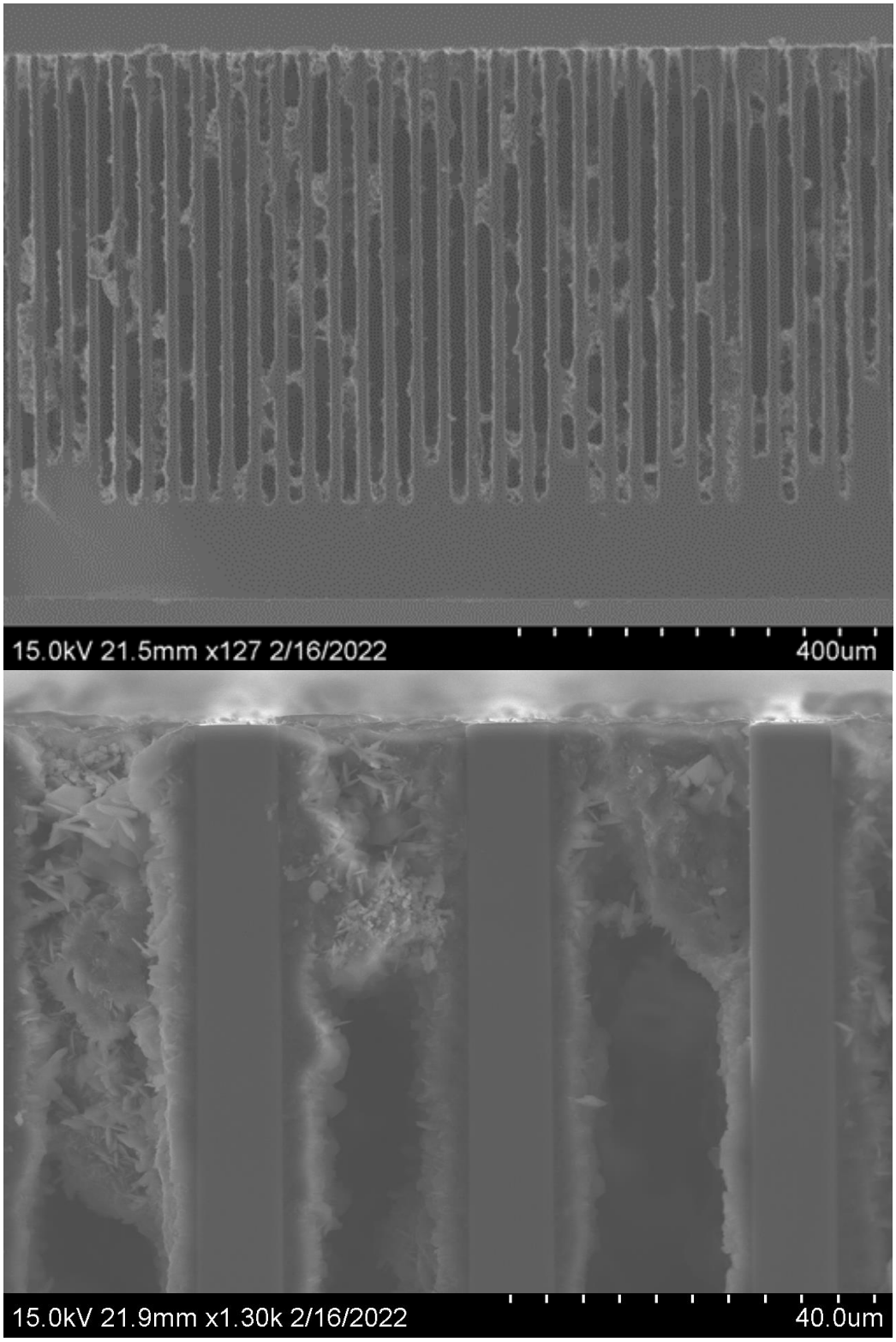

Figure 5-27 - Dendritic growth of Li_2O_2 within the trenches of what was an MSND. The dendrites at the top of the device limited the precipitation of Li_2O_2 within the active volume of the device.

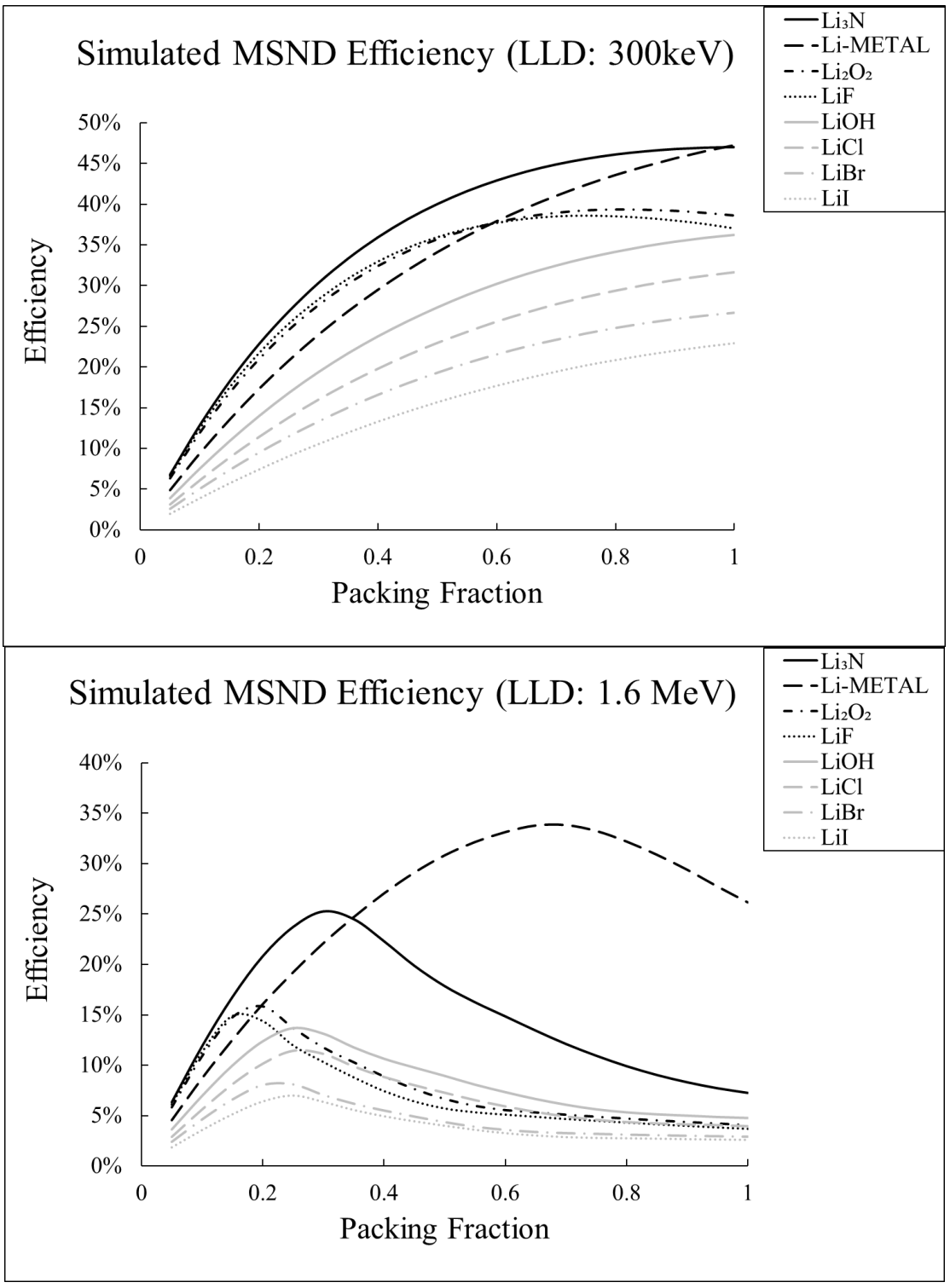

Figure 5-28 - Simulated efficiencies for MSNDs using a pulse-height tally (F8) within MCNP6. Note that the upper yields on efficiencies are dictated by the LLDs. 6LiF, the overall best backfill candidate, performs exceptionally across most packing fractions, is electrically insulating, and does not react chemically with any device materials or moisture.

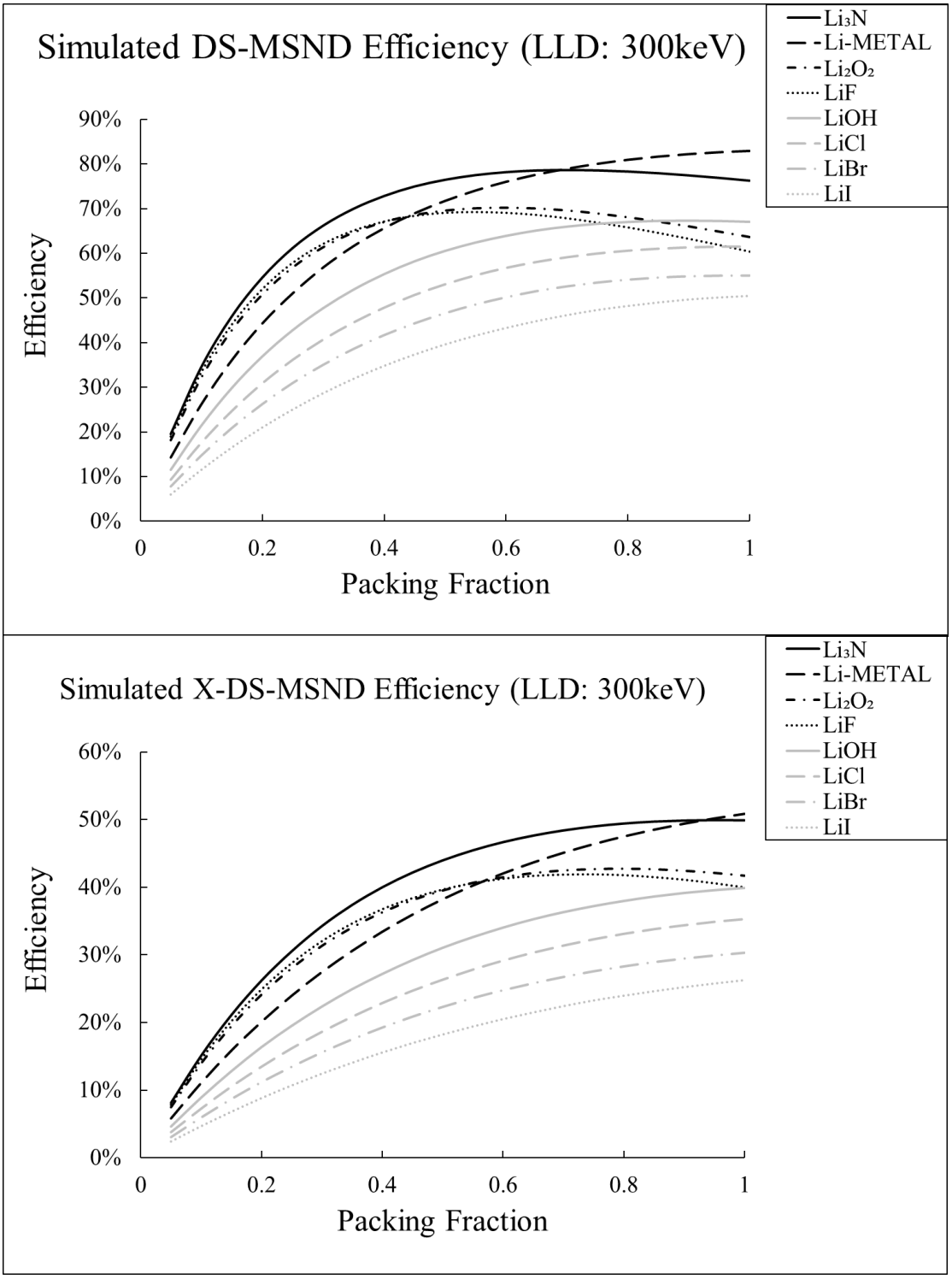

Figure 5-29 - Simulated efficiencies for the double-sided variants of the MSND (DS-MSND and X-DS-MSND). These devices exhibit similar packing-dependent efficiency behavior to MSNDs but utilize the double-sided design to reduce neutron streaming through the fins of the microstructures.

Chapter 6 - Conclusions

Efforts to produce the highest packing fraction backfill yielded limited success within the range of 50-60% - utilizing weighted sonicated techniques or aggressive pressing with a brayer. While weighted sonicated backfills produced negligent damage to the semiconductor diodes, the process results varied heavily as a function of the slurry viscosity, sonicator power, and eventually usage of top-down ^{6}LiF. Aggressive manual pressing with brayers quickly generated high density packing fractions at the cost of higher device failure rate, a result of the constantly evaporating solvent increasing the LiF dispersion viscosity and translating the rolling pressure into horizontal forces that damaged the diodes. The utilization of a low vapor pressure solvent with low viscosity is suggested to be a future milestone as a packing lubricant in the effort to achieve high mechanical packing fractions in MSNDs.

Methods to backfill metallic lithium were unsuccessful. Lithium foil, once heated above 185 ˚C routinely reacted with the bare mechanical specimens, requiring a lithium-passivation material to coat the devices. Studies investigating suitable passivation coatings indicated that parylene would be a suitable compound yet experiments with heated parylene coated samples resulted in wafer destruction, resulting from either parylene reactions (in the case of Par-F) or high CTE behavior of Par-N. Further investigation of metallic lithium backfills will require the thorough identification of which lithium-passivation materials will maintain chemical compatibility with the device, conformally coat the trenches, maintain adhesion to the microstructured silicon substrate, and possess low CTE. Such parameters are expected to enable the backfill of metallic lithium.

Recrystallization of lithium peroxide (a LiF substitute) yielded limited success. The material, while soluble in solvents and water, grows dendritic crystals that result in the bridging (sealing of the tops) of diodes. Attempts to decrease the solvent saturation and limit the "wetting" of the diodes with the solvents resulted in slow crystal growth that occurred along the perimeter of the evaporating solvent. The growth of dendrites was determined to be the limiting factor of this methodology in packing the devices and concerns of the devices chemically reacting over time was mildly satisfied by a solvation test to determine presence of LiOH, yielding less than 10% mass composition of the precipitate as LiOH.

Previous calculations purposing the "ΣL product" as a quantitative tool to designate optimal converter backfills for ^{6}LiF were cross-examined against calculated efficiencies of different ^{6}Li converter materials. These ΣL products were a sufficient designator of which backfill materials would achieve the upper limitations on detection efficiency, as confirmed by pulse height simulation (with LLD) in MSNDs, DS-MSNDs, and X-DS-MSNDs. Backfill comparisons were performed for a library of lithium-based compounds, confirming that the best backfill materials overall are ^{6}LiF and metallic ^{6}Li.

Manufacturing of the MSND involved a proprietary particle "treatment" by RDT to yield acceptable packing fractions (above 40%), and routinely created a manufacturing delay as a result of the treatment (and re-treatment) duration. The findings of this research have yielded a new process for microparticulate preparation that produces a measurable increase for MSND backfill with microparticulate ^{6}LiF, which persists throughout particle recycling.

Bibliography

[1] D. S. McGregor and J. K. Shultis, Radiation Detection: Concepts, Methods, and Devices, Boca Raton: CRC Press, 2020.

[2] J. F. Ziegler, J. P. Biersack and M. D. Ziegler, *The Stopping and Range of Ions in Matter*, www.SRIM.org, 2013.

[3] S. L. Bellinger, "Advanced Microstructured Semiconductor Neutron Detectors: Design, Fabrication, and Performance," PhD Dissertation, Department of Mechanical & Nuclear Engineering, Kansas State University, Manhattan, KS, 2011.

[4] R. G. Fronk, "Dual-Side Etched Microstructured Semiconductor Neutron Detectors," PhD Dissertation, Department of Mechanical & Nuclear Engineering, Kansas State University, Manhattan, KS, 2011.

[5] T. R. Ochs, "Advanced Dual-Sided Microstructured Semiconductor Neutron Detectors," PhD Dissertation, Department of Mechanical & Nuclear Engineering, Kansas State University, Manhattan, KS, 2020.

[6] B. Montag, "Lithiated Ternary Compounds for Neutron Detectors: Material Production and Device Characterization of Lithium Zinc Phosphide and Lithium Zinc Arsenide," PhD Dissertation, Department of Mechanical & Nuclear Engineering, Kansas State University, Manhattan, KS, 2015.

[7] B. Robertson, S. Adenwalla and A. Harken, "A Class of Boron-Rich Solid-State Neutron Detectors," *App. Phys. Letters*, vol. 80, no. 19, pp. 3644-3646, 2002.

[8] D. McGregor and J. Shultis, "Efficiencies of Coated and Perforated Semiconductor Neutron Detectors," in *IEEE Symposium*, Rome, 2004.

[9] R. Muminov and L. Tsvang, "High Efficiency Semiconductor Thermal-Neutron Detectors," *Sov. At. Energy*, vol. 62, pp. 316-319, 1987.

[10] T. R. Ochs, R. G. Fronk, S. L. Bellinger and D. S. McGregor, "Design and Performance Considerations for Dual-Sided Microstructured Semiconductor Neutron Detectors," *Nuc. Inst. and Meth. in Phys. Research, A*, vol. 951, 2019.

[11] D. S. McGregor, S. L. Bellinger and J. K. Shultis, "Present Status of Microstructured Semiconductor Neutron Detectors," *Journal of Cryst. Growth*, vol. 379, pp. 99-110, 2013.

[12] C. B. Stubblefield and R. O. Bach, "Solubility of Lithium Fluoride in Water," *Chem. and Eng. Data*, vol. 17, no. 4, pp. 491-492, 1972.

[13] D. A. Wynn, M. M. Roth and B. D. Pollard, "The Solubility of Alkali-Metal Fluorides in Non-aqueous Solvents with and without Crown Ethers, as Determined by Flame Emission Spectrometry," *Talanta,* vol. 31, no. 11, pp. 1036-1040, 1984.

[14] N. Xin, Y. Sun, M. He, C. Radke and J. Prausnitz, "Solubilities of Six Lithium Salts in Five Non-Aqueous Solvents and in a Few of Their Binary Mixtures," *Fluid Phase Equilibria,* vol. 461, no. 15, pp. 1-7, 2018.

[15] R. Sarraf-Mamoory and N. Rahi-Noori, "The Effect of Precipitation Parameters on Preparation of Lithium Fluoride (LiF) Nano-powder," *Chem. Eng. Comm.,* vol. 194, pp. 1022-1028, 2007.

[16] J. Jindra, "The Preparation of Crystalline Lithium Fluoride by Controlled Precipitation," *Cryst. Tech.,* pp. 69-75, 1969.

[17] D. A. Boryta, "Solubility of Lithium Bromide in Water Between -50 °C and +100 °C (45 to 70% Lithium Bromide)," *J. Chem. Eng. Data,* vol. 15, no. 1, pp. 142-144, 1970.

[18] X. Wu, Y. Gong, S. Xu, Z. Yan, X. Zhang and S. Yang, "Electrical Conductivity of Lithium Chloride, Lithium Bromide, and Lithium Iodide Electrolytes in Methanol, Water, and Their Binary Mixtures," *American Chem. Soc.,* vol. 64, no. 10, pp. 4319-4329, 2019.

[19] A. Seidell and W. F. Linke, "Solubilities of Inorganic and Organic Compounds: A Compilation of Solubility Data from the Periodical Literature," *Chem. Ed.,* 1952.

[20] D. J. Diamond, "The Efficiency of Neutron Detection with a Lithium Iodide, Europium Activated, Scintillation Crystal.," MS Thesis, Department of Nuclear Engineering, University of Arizona, Tuscon, Arizona, 1963.

[21] A. B. Charette, Encyc. Reag. for Organic Synth., 2001.

[22] M. Gutsche, H. Seidl, T. Hecht, S. Kudelka and U. Schroeder, "Atomic Layer Deposition for Advanced DRAM Applications," Fut. Fab. International, 2003.

[23] Y. Lee, H. Sun, M. Young and S. George, "Atomic Layer Deposition of Metal Fluorides Using HF-Pyridine as the Fluorine Precursor," *Chem. Mater.,* vol. 28, pp. 2022-2032, 2016.

[24] A. Mane, J. Libera and J. Elam, "Atomic Layer Deposition of LiF Thin Films Using Lithium Tert-butoxide and Metal Fluoride Precursors," in *16th Int. Conf. on Atomic Layer Dep.,* Dublin, Ireland, 2016 (July 24-27).

[25] M. Mäntymäki, J. Hämäläinen, E. Puukilainen, T. Sajavaara, M. Ritala and M. Leskelä, "Atomic Layer Deposition of LiF Thin Films from Lithd, Mg(thd)2, and TiF4 Precursors," *Chem. Mater.,* vol. 25, pp. 1656-1663, 2013.

[26] M. Mäntymäki, M. Ritala and M. Leskelä, "Metal Fluorides as Lithium-Ion Battery Materials: An Atomic Layer Deposition Perspective," *Coatings,* vol. 8, no. 277, 2018.

[27] J. Wank, S. George and A. Weimer, "Nanocoating Individual Cohesive Boron Nitride Particles in a Fluidized Bed by ALD," *Powd. Tech.,* vol. 142, no. 1, pp. 59-69, 2004.

[28] M. Saito, T. Ueda and T. Tani, "Process for Preparing B-Diketone Compound and Process for Preparing Metal Complex Thereof". International Patent (PCT) Patent WO 03/059858 A2, 24 July 2003.

[29] R. C. Morrison, C. W. Kamienski and J. A. Schwindeman, "Method of Preparation of Lithium Tertiary-Butoxide". United States Patent 5,583,269, 8 May 1995.

[30] "Material Deposition Chart," Kurt J. Lesker, [Online]. Available: https://www.lesker.com/newweb/deposition_materials/materialdepositionchart.cfm?pgid=0. [Accessed 2022].

[31] P. Siemroth, C. Wenzel, W. Klimes, B. Schultrich and T. Schulke, "Metallization of Sub-micron Trenches and Vias with High Aspect Ratio," *Thin Solid Films,* Vols. 308-309, pp. 455-459, 1997.

[32] J. Jones, M. Anouti and M. Caillon-Caravanier, "Thermodynamic of LiF Dissolution in Alkylcarbonates and Some of Their Mixtures with Water," *Fluid Phase Eq.,* vol. 282, pp. 62-68, 2009.

[33] W. McNeil, "Perforated Diode Neutron Sensors," PhD Dissertation, Department of Mechanical & Nuclear Engineering, Kansas State University, Manhattan, KS, 2010.

[34] I. Lifshitz and V. Slyozov, "The Kinetics of Precipitation From Supersaturated Solid Solutions," *Phys. and Chem. of Solids,* vol. 19, no. 1-2, pp. 35-50, 1961.

[35] D. Legland, I. Arganda-Carreras and P. Andrey, "MorphoLibJ: Integrated Library and Plugins for Mathematical Morphology with ImageJ," *Bioinformatics,* vol. 32, no. 22, pp. 3532-3534, 2016.

[36] R. German, Particle Packing Characteristics, Princeton: Metal Powder Industries Federation, 1989.

[37] D. Buckley, "Influence of Surface Active Agents on Friction, Deformation, and Fracture of Lithium Fluoride," NASA, Cleveland, 1968.

[38] E. Logtenberg and H. Stein, "Zeta Potential And Coagulation of ZnO In Alcohols," *Colloids and Surf.,* vol. 17, pp. 305-312, 1985.

[39] S. Pethaiah, K. Sadasivuni, A. Jayakumar, D. Ponnamma, C. Tiwary and G. Sasikumar, "Methanol Electrolysis for Hydrogen Production Using Polymer Electrolyte Membrane: A Mini-Review," *Energies,* vol. 13, pp. 5879-5896, 2020.

[40] W. Wang, "Super-Conformal Coatings and Filling of High Aspect Ratio Recessed Structures by Two-Molecule CVD," 2014.

[41] J. Xie, A. Sendek, E. Cubuk, X. Zhang, Z. Lu, Y. Gong, T. Wu, F. Shi, W. Liu, E. Reed and et al., "Atomic Layer Deposition of Stable LiAlF4 Lithium Ion Conductive Interfacial Layer for Stable Cathode Cycling," *ACS Nano,* vol. 11, pp. 7019-7027, 2017.

[42] M. Mäntymäki, J. Hämäläinen, E. Puukilainen, F. Munnik, M. Ritala and M. Leskelä, "Atomic Layer Deposition of LiF Thin Films from Lithd and TiF4 Precursors," *Chem. Vap. Depos.,* vol. 19, pp. 111-116, 2013.

[43] A. Charette, J. Barbay and H. Wei, "Lithium Iodide," in *Encyclopedia of Reagents for Organic Synthesis*, Wiley, 2006.

[44] C. Stubblefield and R. Bach, "Solubility of Lithium Fluoride in Water," *J. Chem. Eng. Data,* vol. 17, no. 4, pp. 491-492, 1972.

[45] D. A. Boryta, "Solubility of Lithium Bromide in Water between -50 and +100C (45 to 70% Lithium Bromide)," *Chemical and Eng. Data,* vol. 15, no. 1, pp. 142-144, 1970.

[46] C. Schneider, W. Rasband and K. Eliceiri, "NIH Image to ImageJ: 25 Years of Image Analysis," *Nature Methods,* vol. 9, pp. 671-675, 2012.

[47] B. Van Der Hoff and G. Benson, "A Quantum-Mechanical Calculation of the Surface Energy of Crystalline Lithium Fluoride," *Journal of Chem. Phys.,* vol. 22, no. 3, pp. 475-480, 1954.

[48] A. Mazzoli and O. Favoni, "Particle Size, Size Distribution and Mophological Evaluation of Airborne Dust Particles of Diverse Woods by Scanning Electron Microscopy and Image Processing Program," *Powder Technology,* vol. 225, pp. 65-72, 2012.

[49] e. a. D. A. Brown, "The 8th Major Release of the Nuclear Reaction Data LIbrary with CIELO-Project Cross Sections, New Standards and Thermal Scattering Data," *Nuc. Data Sheets,* vol. 148, 2018.

Appendix A - C++ Automation of Iterative MCNP Calculations

```
// Incrementally modify MCNP input file density value (and material number), run MCNP6, delete runtpe, and
prepare pulse height tallies for output

#include <iostream>
#include <fstream>
#include <string>
#include <Windows.h>
#include "mcncpp_lib.h"


using namespace std;

// initialize global variables
string mat_den;
string name;
string out;
string data_read;
string bucket_data;
string bucket_error;
string runline;

string alpha_holder[20][8];
string triton_holder[20][8];
string comb_holder[20][8];

int locator = 0;
// find occurence of tally based on "##________nps" format for a 2 digit integer, 8 spaces, and "nps".  Skip 9 lines.
Output data.
string datafinder(int num, std::ifstream &file_name, int skip) {

    // setup string to search for
    string target_data;
    string results;
    string snipper;

    // convert function argument int to a string with the known format of occurance in mcnp output file
    target_data.append("1tally       ");
    target_data.append(to_string(num));
    target_data.append("        nps =     1000000");


    // setup container string and bool found condition
    string haystack;
    bool located = 0;
    file_name.clear();
    file_name.seekg(0);
    // getline from document until item is found
    while (located == FALSE){
        getline(file_name, haystack);
        if (haystack.find(target_data) != string::npos) {
            located = TRUE;
```

```
        }
    }

    // skip N lines and prepare for output just in case
    for (int z = 1; z <= (skip + 1); z++) {
        getline(file_name, snipper);

    }
    results.append(snipper);

    // return final output string
    return results;

}

// construct DS-MSND MCNP input file with designated material number/density and file name
void write_new_dsmsnd_inputfile(string input_line, string fname) {
    ofstream output;
    output.open(fname);
    output << "c
==========================================================================="
<< endl;
    output << "c       Investigation of Alpha and Triton Ranges in LiF Substitutes"                << endl;
    output << "c
==========================================================================="
<< endl;
    output << "c                              Cell Cards"                                  << endl;
    output << "c
==========================================================================="
<< endl;
    output << "10 100 -2.329     -10                u=1                $ Frontside fin" << endl;
    output << "11 " << input_line << "      10           u=1              $ Frontside trench" << endl;
    output << "12 0           -11       lat=1 fill=1 u=2            $ Frontside unit cell" << endl;
    output << "13 0           -12            fill=2                   $ Front Diode" << endl;
    output << "14 100 -2.329     -13 12 14                    $ Between front/back sides" << endl;
    output << "15 100 -2.329     -16                u=3                $ Backside fin" << endl;
    output << "16 " << input_line << "      16           u=3              $ Backside trench" << endl;
    output << "17 0           -15       lat=1 fill=3 u=4            $ Backside unit cell" << endl;
    output << "18 0           -14            fill=4                   $ Backside Diode" << endl;
    output << "C World" << endl;
    output << "100 0 #13 #14 #18 -100 $ VOID IN WORLD" << endl;
    output << "101 0 100 $ OUTSIDE WORLD" << endl;
    output << "" << endl;
    output << "C ===================================================================" <<
endl;
    output << "C --------------------SURFACE CARDS-----------------" << endl;
    output << "C ===================================================================" <<
endl;
    output << "C DSMSND" << endl;
    output << "c      x-min  x-max   y-min  y-max   z-min  z-max" << endl;
    output << "10 RPP -0.5000 0.5000 -0.0005 0.0005 0.0000 0.0600 $ Front Sidewall" << endl;
    output << "11 RPP -0.5000 0.5000 -0.0015 0.0015 0.0000 0.0600 $ Front Unit Cell" << endl;
    output << "12 RPP -0.5000 0.5000 -0.5000 0.5000 0.0000 0.0600 $ Front Diode" << endl;
    output << "13 RPP -0.5000 0.5000 -0.5000 0.5000 0.0600 0.0900 $ Middle of Diode" << endl;
    output << "14 RPP -0.5000 0.5000 -0.5000 0.5000 0.0900 0.1500 $ Backside Diode" << endl;
    output << "15 RPP -0.5000 0.5000  0.0000 0.0030 0.0900 0.1500 $ Backside Unit Cell" << endl;
```

```
   output << "16 RPP -0.5000 0.5000  0.0010 0.0020 0.0900 0.1500 $ Backside Sidewall" << endl;
   output << "C" << endl;
   output << "100 so 50 $ universe" << endl;
   output << " "                                                    << endl;
   output << "c
==========================================================================="
<< endl;
   output << "c                          Data Cards"                          << endl;
   output << "c
==========================================================================="
<< endl;
   output << "c
==========================================================================" <<
endl;
   output << "c                          Data Cards" << endl;
   output << "c
==========================================================================" <<
endl;
   output << "c             Monodirectional Watt Spectrum Neutron Source" << endl;
   output << "c _____________________________________________________________________________"
<< endl;
   output << "SDEF POS=0 0 -1 X=d1 Y=d2 Z=-0.2  PAR=1   ERG=2.5E-8 VEC=0 0 1 DIR=1" << endl;
   output << "SI1 -0.5 0.5                  $sample range Xmin to Xmax : -0.5cm to 0.5cm" << endl;
   output << "SP1 0   1                       $weighting for x sampling: here constant" << endl;
   output << "SI2 -0.5 0.5                  $sample range Ymin to Ymax : -0.5cm to 0.5cm" << endl;
   output << "SP2 0   1                       $weighting for y sampling: here constant" << endl;
   output << "c SP3 -3 1.180 1.03419            $watt fission spectrum pg 11-4 MCNP6 manual" << endl;
   output << "c ---------------------------------------------------------------------------" << endl;
   output << "c                       Physics Cards" << endl;
   output << "c _____________________________________________________________________________"
<< endl;
   output << "MODE: N T A E P       $enable physics to transport neutrons tritons and alphas" << endl;
   output << "IMP:N 1 9R 0           $importance for neutrons in cells - in order of cells" << endl;
   output << "IMP:A 1 9R 0            $importance for alphas in cells - in order of cells" << endl;
   output << "IMP:T 1 9R 0           $importance for tritons in cells - in order of cells" << endl;
   output << "IMP:E 1 9R 0           $importance for tritons in cells - in order of cells" << endl;
   output << "IMP:P 1 9R 0           $importance for tritons in cells - in order of cells" << endl;
   output << "PHYS:N 6J 3          $use NCIA for neutron capture ion algorithm for sampling" << endl;
   output << "CUT:N 2J 0                                    $neutron cutoff" << endl;
   output << "CUT:A J 0.01 0                                  $alpha cutoff" << endl;
   output << "CUT:T J 0.01 0                                 $triton cutoff" << endl;
   output << "NPS 1E6                             $run for X neutron histories" << endl;
   output << "c STOP F18 0.01       $stop sim when all bins in tally F28 are RE 0.01 or less" << endl;
   output << "c PRDMP 5E4                           $print out every 5E4 histories" << endl;
   output << "c ---------------------------------------------------------------------------" << endl;
   output << "c                       Tally Cards" << endl;
   output << "c _____________________________________________________________________________"
<< endl;
   output << "F18:T,A,E,P  10 15                              $Comb TA tally" << endl;
   output << "E18 0 0.3 5                        $energy bins for comb TA tally" << endl;
   output << "F28:A    10 15                                  $Alpha tally" << endl;
   output << "E28 0 0.3 5                       $energy bins for comb alpha tally" << endl;
   output << "F38:T    10 15                                 $Triton tally" << endl;
   output << "E38 0 0.3 5                      $energy bins for comb triton tally" << endl;
   output << "F48:T,A,E,P  10 15                              $Comb TA tally" << endl;
   output << "E48 0 1.6 5                        $energy bins for comb TA tally" << endl;
```

```
   output << "F58:A    10 15                                  $Alpha tally" << endl;
   output << "E58 0 1.6 5                              $energy bins for comb alpha tally" << endl;
   output << "F68:T    10 15                                  $Triton tally" << endl;
   output << "E68 0 1.6 5                              $energy bins for comb triton tally" << endl;
   output << "c
=============================================================================" <<
endl;
   output << "c                          Material Cards" << endl;
   output << "c
=============================================================================" <<
endl;
   output << "c" << endl;
   output << "c ///////////////////////////////////////////////////////////////////////////" << endl;
   output << "c                 LiF   rho= 2.546 g/cc    95pct_wt Li6 Enrichment" << endl;
   output << "c ///////////////////////////////////////////////////////////////////////////" << endl;
   output << "m1      3006    0.95" << endl;
   output << "        3007    0.05" << endl;
   output << "        9018    1" << endl;
   output << "c" << endl;
   output << "c ///////////////////////////////////////////////////////////////////////////" << endl;
   output << "c              Metallic-Li   rho= 0.46682 g/cc    95pct_wt Li6 Enrichment" << endl;
   output << "c ///////////////////////////////////////////////////////////////////////////" << endl;
   output << "m2      3006    0.95" << endl;
   output << "        3007    0.05" << endl;
   output << "c" << endl;
   output << "c ///////////////////////////////////////////////////////////////////////////" << endl;
   output << "c               LiCl   rho= 2.025464 g/cc    95pct_wt Li6 Enrichment" << endl;
   output << "c ///////////////////////////////////////////////////////////////////////////" << endl;
   output << "m3      3006    0.95" << endl;
   output << "        3007    0.05" << endl;
   output << "        17035   0.75770" << endl;
   output << "        17037   0.24230" << endl;
   output << "c" << endl;
   output << "c ///////////////////////////////////////////////////////////////////////////" << endl;
   output << "c              LiOH   rho= 1.406227313 g/cc    95pct_wt Li6 Enrichment" << endl;
   output << "c ///////////////////////////////////////////////////////////////////////////" << endl;
   output << "c" << endl;
   output << "m4      1001    1" << endl;
   output << "        3006    0.95" << endl;
   output << "        3007    0.05" << endl;
   output << "        8016    1" << endl;
   output << " c" << endl;
   output << "c ///////////////////////////////////////////////////////////////////////////" << endl;
   output << "c              LiBr   rho= 3.429046674 g/cc    95pct_wt Li6 Enrichment" << endl;
   output << "c ///////////////////////////////////////////////////////////////////////////" << endl;
   output << "c" << endl;
   output << "m5      3006    0.95" << endl;
   output << "        3007    0.05" << endl;
   output << "        35079   0.5069" << endl;
   output << "        35081   0.4931" << endl;
   output << "c" << endl;
   output << "c ///////////////////////////////////////////////////////////////////////////" << endl;
   output << "c              Li3N   rho= 1.174173185 g/cc    95pct_wt Li6 Enrichment" << endl;
   output << "c ///////////////////////////////////////////////////////////////////////////" << endl;
   output << "c" << endl;
   output << "m6      3006    2.85" << endl;
```

```
    output << "        3007    0.15" << endl;
    output << "        7014    1" << endl;
    output << "c" << endl;
    output << "c ////////////////////////////////////////////////////////////////////////////" << endl;
    output << "c               LiI   rho= 4.049191185 g/cc    95pct_wt Li6 Enrichment" << endl;
    output << "c ////////////////////////////////////////////////////////////////////////////" << endl;
    output << "c" << endl;
    output << "m7      3006    0.95" << endl;
    output << "        3007    0.05" << endl;
    output << "        53127   1" << endl;
    output << "c" << endl;
    output << "c ////////////////////////////////////////////////////////////////////////////" << endl;
    output << "c               Li2O2   rho= 2.221346057 g/cc    95pct_wt Li6 Enrichment" << endl;
    output << "c ////////////////////////////////////////////////////////////////////////////" << endl;
    output << "c" << endl;
    output << "m8      3006    0.95" << endl;
    output << "        3007    0.05" << endl;
    output << "        8016    1" << endl;
    output << "c" << endl;
    output << "c ////////////////////////////////////////////////////////////////////////////" << endl;
    output << "c                 Si   rho= 2.329 g/cc    95pct_wt Li6 Enrichment" << endl;
    output << "c ////////////////////////////////////////////////////////////////////////////" << endl;
    output << "m100    14028.70c   922" << endl;
    output << "        14029.70c   47" << endl;
    output << "        14030.70c   31" << endl;
    output.close();
}

// construct X-DS-MSND MCNP input file with designated material number/density and file name
void write_new_xdsmsnd_inputfile(string input_line, string fname) {
    ofstream output;
    output.open(fname);
    output << "c
================================================================================" <<
endl;
    output << "c       Investigation of Alpha and Triton Ranges in LiF Substitutes" << endl;
    output << "c
================================================================================" <<
endl;
    output << "c                              Cell Cards" << endl;
    output << "c
================================================================================" <<
endl;
    output << "10 100 -2.329     -10                u=1                  $ Frontside fin" << endl;
    output << "11 " << input_line << "      10           u=1                $ Frontside trench" << endl;
    output << "12 0           -11       lat=1 fill=1 u=2             $ Frontside unit cell" << endl;
    output << "13 0           -12             fill=2                   $ Front Diode" << endl;
    output << "14 100 -2.329     -13 12 14                    $ Between front/back sides" << endl;
    output << "15 100 -2.329     -16                u=3                  $ Backside fin" << endl;
    output << "16 " << input_line << "      16           u=3              $ Backside trench" << endl;
    output << "17 0           -15       lat=1 fill=3 u=4             $ Backside unit cell" << endl;
    output << "18 0           -14             fill=4                   $ Backside Diode" << endl;
    output << "C World" << endl;
    output << "100 0 #13 #14 #18 -100 $ VOID IN WORLD" << endl;
    output << "101 0 100 $ OUTSIDE WORLD" << endl;
    output << "" << endl;
```

```
   output << "C ================================================================" <<
endl;
   output << "C ----------SURFACE CARDS----------" << endl;
   output << "C ================================================================" <<
endl;
   output << "C DSMSND" << endl;
   output << "c      x-min  x-max   y-min  y-max   z-min  z-max" << endl;
   output << "10 RPP -0.7882 0.7882 -0.00135 0.00135 0.0000 0.0450 $ Front Sidewall" << endl;
   output << "11 RPP -0.7882 0.7882 -0.0014  0.0014  0.0000 0.0450 $ Front Unit Cell" << endl;
   output << "12 RPP -0.7882 0.7882 -0.70675 0.70675 0.0000 0.0450 $ Front Diode" << endl;
   output << "13 RPP -0.7882 0.7882 -0.70675 0.70675 0.0450 0.0850 $ Middle of Diode" << endl;
   output << "14 RPP -0.7882 0.7882 -0.70675 0.70675 0.0850 0.1300 $ Backside Diode" << endl;
   output << "15 RPP -0.7882 0.7882  0.0000  0.0030  0.0850 0.1300 $ Backside Unit Cell" << endl;
   output << "16 RPP -0.7882 0.7882  0.0010  0.0020  0.0850 0.1300 $ Backside Sidewall" << endl;
   output << "C" << endl;
   output << "100 so 50 $ universe" << endl;
   output << " " << endl;
   output << "c
============================================================================" <<
endl;
   output << "c                          Data Cards" << endl;
   output << "c
============================================================================" <<
endl;
   output << "c
============================================================================" <<
endl;
   output << "c                          Data Cards" << endl;
   output << "c
============================================================================" <<
endl;
   output << "c             Monodirectional Watt Spectrum Neutron Source" << endl;
   output << "c ____________________________________________________________________________"
<< endl;
   output << "SDEF POS=0 0 -1 X=d1 Y=d2 Z=-0.2  PAR=1   ERG=2.5E-8 VEC=0 0 1 DIR=1" << endl;
   output << "SI1 -0.5 0.5                  $sample range Xmin to Xmax : -0.5cm to 0.5cm" << endl;
   output << "SP1 0   1                       $weighting for x sampling: here constant" << endl;
   output << "SI2 -0.5 0.5                  $sample range Ymin to Ymax : -0.5cm to 0.5cm" << endl;
   output << "SP2 0   1                       $weighting for y sampling: here constant" << endl;
   output << "c SP3 -3 1.180 1.03419             $watt fission spectrum pg 11-4 MCNP6 manual" << endl;
   output << "c ----------------------------------------------------------------------------" << endl;
   output << "c                       Physics Cards" << endl;
   output << "c ____________________________________________________________________________"
<< endl;
   output << "MODE: N T A E P        $enable physics to transport neutrons tritons and alphas" << endl;
   output << "IMP:N 1 9R 0           $importance for neutrons in cells - in order of cells" << endl;
   output << "IMP:A 1 9R 0            $importance for alphas in cells - in order of cells" << endl;
   output << "IMP:T 1 9R 0           $importance for tritons in cells - in order of cells" << endl;
   output << "IMP:E 1 9R 0           $importance for tritons in cells - in order of cells" << endl;
   output << "IMP:P 1 9R 0           $importance for tritons in cells - in order of cells" << endl;
   output << "PHYS:N 6J 3          $use NCIA for neutron capture ion algorithm for sampling" << endl;
   output << "CUT:N 2J 0                                        $neutron cutoff" << endl;
   output << "CUT:A J 0.01 0                                     $alpha cutoff" << endl;
   output << "CUT:T J 0.01 0                                    $triton cutoff" << endl;
   output << "NPS 1E6                              $run for X neutron histories" << endl;
   output << "c STOP F18 0.01       $stop sim when all bins in tally F28 are RE 0.01 or less" << endl;
```

```
   output << "c PRDMP 5E4                              $print out every 5E4 histories" << endl;
   output << "c ------------------------------------------------------------------------------" << endl;
   output << "c                          Tally Cards" << endl;
   output << "c ____________________________________________________________________________________"
<< endl;
   output << "F18:T,A,E,P  10 15                                  $Comb TA tally" << endl;
   output << "E18 0 0.3 5                               $energy bins for comb TA tally" << endl;
   output << "F28:A    10 15                                  $Alpha tally" << endl;
   output << "E28 0 0.3 5                              $energy bins for comb alpha tally" << endl;
   output << "F38:T    10 15                                 $Triton tally" << endl;
   output << "E38 0 0.3 5                             $energy bins for comb triton tally" << endl;
   output << "F48:T,A,E,P  10 15                                  $Comb TA tally" << endl;
   output << "E48 0 1.6 5                               $energy bins for comb TA tally" << endl;
   output << "F58:A    10 15                                  $Alpha tally" << endl;
   output << "E58 0 1.6 5                              $energy bins for comb alpha tally" << endl;
   output << "F68:T    10 15                                 $Triton tally" << endl;
   output << "E68 0 1.6 5                             $energy bins for comb triton tally" << endl;
   output << "c
==========================================================================" <<
endl;
   output << "c                          Material Cards" << endl;
   output << "c
==========================================================================" <<
endl;
   output << "c" << endl;
   output << "c ////////////////////////////////////////////////////////////////////////////" << endl;
   output << "c                 LiF   rho= 2.546 g/cc    95pct_wt Li6 Enrichment" << endl;
   output << "c ////////////////////////////////////////////////////////////////////////////" << endl;
   output << "m1      3006    0.95" << endl;
   output << "        3007    0.05" << endl;
   output << "        9018    1" << endl;
   output << "c" << endl;
   output << "c ////////////////////////////////////////////////////////////////////////////" << endl;
   output << "c               Metallic-Li   rho= 0.46682 g/cc    95pct_wt Li6 Enrichment" << endl;
   output << "c ////////////////////////////////////////////////////////////////////////////" << endl;
   output << "m2      3006    0.95" << endl;
   output << "        3007    0.05" << endl;
   output << "c" << endl;
   output << "c ////////////////////////////////////////////////////////////////////////////" << endl;
   output << "c                LiCl   rho= 2.025464 g/cc    95pct_wt Li6 Enrichment" << endl;
   output << "c ////////////////////////////////////////////////////////////////////////////" << endl;
   output << "m3      3006    0.95" << endl;
   output << "        3007    0.05" << endl;
   output << "        17035   0.75770" << endl;
   output << "        17037   0.24230" << endl;
   output << "c" << endl;
   output << "c ////////////////////////////////////////////////////////////////////////////" << endl;
   output << "c               LiOH   rho= 1.406227313 g/cc    95pct_wt Li6 Enrichment" << endl;
   output << "c ////////////////////////////////////////////////////////////////////////////" << endl;
   output << "c" << endl;
   output << "m4      1001    1" << endl;
   output << "        3006    0.95" << endl;
   output << "        3007    0.05" << endl;
   output << "        8016    1" << endl;
   output << " c" << endl;
   output << "c ////////////////////////////////////////////////////////////////////////////" << endl;
```

```
    output << "c              LiBr   rho= 3.429046674 g/cc    95pct_wt Li6 Enrichment" << endl;
    output << "c ////////////////////////////////////////////////////////////////////////////" << endl;
    output << "c" << endl;
    output << "m5     3006    0.95" << endl;
    output << "       3007    0.05" << endl;
    output << "       35079   0.5069" << endl;
    output << "       35081   0.4931" << endl;
    output << "c" << endl;
    output << "c ////////////////////////////////////////////////////////////////////////////" << endl;
    output << "c              Li3N   rho= 1.174173185 g/cc    95pct_wt Li6 Enrichment" << endl;
    output << "c ////////////////////////////////////////////////////////////////////////////" << endl;
    output << "c" << endl;
    output << "m6     3006    2.85" << endl;
    output << "       3007    0.15" << endl;
    output << "       7014    1" << endl;
    output << "c" << endl;
    output << "c ////////////////////////////////////////////////////////////////////////////" << endl;
    output << "c              LiI   rho= 4.049191185 g/cc    95pct_wt Li6 Enrichment" << endl;
    output << "c ////////////////////////////////////////////////////////////////////////////" << endl;
    output << "c" << endl;
    output << "m7     3006    0.95" << endl;
    output << "       3007    0.05" << endl;
    output << "       53127   1" << endl;
    output << "c" << endl;
    output << "c ////////////////////////////////////////////////////////////////////////////" << endl;
    output << "c              Li2O2   rho= 2.221346057 g/cc    95pct_wt Li6 Enrichment" << endl;
    output << "c ////////////////////////////////////////////////////////////////////////////" << endl;
    output << "c" << endl;
    output << "m8     3006    0.95" << endl;
    output << "       3007    0.05" << endl;
    output << "       8016    1" << endl;
    output << "c" << endl;
    output << "c ////////////////////////////////////////////////////////////////////////////" << endl;
    output << "c                Si   rho= 2.329 g/cc    95pct_wt Li6 Enrichment" << endl;
    output << "c ////////////////////////////////////////////////////////////////////////////" << endl;
    output << "m100    14028.70c   922" << endl;
    output << "       14029.70c   47" << endl;
    output << "       14030.70c   31" << endl;
    output.close();
}

// construct MSND MCNP input file with designated material number/density and file name
void write_new_msnd_inputfile(string input_line, string fname) {
    ofstream output;
    output.open(fname);
    output << "C ============================================================" << endl;
    output << "C -------------------CELL CARD-------------------------------" << endl;
    output << "C ============================================================" << endl;
    output << "10 100 -2.329     -10                  u=1                 $ Frontside fin" << endl;
    output << "11 " << input_line << " 10             u=1                $ Frontside trench" << endl;
    output << "12 0           -11        lat=1 fill=1 u=2             $ Frontside unit cell" << endl;
    output << "13 0           -12             fill=2                  $ Front Diode" << endl;
    output << "14 100 -2.329     -13                                    $ Base of Diode" << endl;
    output << "C World" << endl;
    output << "100 0 #13 #14 -100                                      $ VOID IN WORLD" << endl;
    output << "101 0 100                                               $ GRAVEYARD" << endl;
```

```
   output << "" << endl;
   output << "C ================================================================" <<
endl;
   output << "C ----------SURFACE CARDS----------" << endl;
   output << "C ================================================================" <<
endl;
   output << "C MSND" << endl;
   output << "c      x-min  x-max   y-min  y-max   z-min  z-max" << endl;
   output << "10 RPP  -0.5000 0.5000 -0.0005 0.0005 0.0000 0.0500$ Front Sidewall" << endl;
   output << "11 RPP  -0.5000 0.5000 -0.0015 0.0015 0.0000 0.0500$ Front Unit Cell" << endl;
   output << "12 RPP  -0.5000 0.5000 -0.5000 0.5000 0.0000 0.0400$ Front Diode" << endl;
   output << "13 RPP  -0.5000 0.5000 -0.5000 0.5000 0.0400 0.0600$ Base of Diode" << endl;
   output << "C" << endl;
   output << "100 so 50 $ universe" << endl;
   output << "" << endl;
   output << "C ================================================================="
<< endl;
   output << "C ----------DATA CARDS----------" << endl;
   output << "C ================================================================="
<< endl;
   output << "C" << endl;
   output << "c
================================================================================" <<
endl;
   output << "c                          Data Cards" << endl;
   output << "c
================================================================================" <<
endl;
   output << "c              Monodirectional Watt Spectrum Neutron Source" << endl;
   output << "c ____________________________________________________________________________"
<< endl;
   output << "SDEF POS=0 0 -1 X=d1 Y=d2 Z=-0.2  PAR=1   ERG=2.5E-8 VEC=0 0 1 DIR=1" << endl;
   output << "SI1 -0.5 0.5                  $sample range Xmin to Xmax : -0.5cm to 0.5cm" << endl;
   output << "SP1 0   1                       $weighting for x sampling: here constant" << endl;
   output << "SI2 -0.5 0.5                  $sample range Ymin to Ymax : -0.5cm to 0.5cm" << endl;
   output << "SP2 0   1                       $weighting for y sampling: here constant" << endl;
   output << "c SP3 -3 1.180 1.03419             $watt fission spectrum pg 11-4 MCNP6 manual" << endl;
   output << "c ----------" << endl;
   output << "c                        Physics Cards" << endl;
   output << "c ____________________________________________________________________________"
<< endl;
   output << "MODE: N T A E P        $enable physics to transport neutrons tritons and alphas" << endl;
   output << "IMP:N 1 5R 0            $importance for neutrons in cells - in order of cells" << endl;
   output << "IMP:A 1 5R 0             $importance for alphas in cells - in order of cells" << endl;
   output << "IMP:T 1 5R 0            $importance for tritons in cells - in order of cells" << endl;
   output << "IMP:E 1 5R 0            $importance for tritons in cells - in order of cells" << endl;
   output << "IMP:P 1 5R 0            $importance for tritons in cells - in order of cells" << endl;
   output << "PHYS:N 6J 3           $use NCIA for neutron capture ion algorithm for sampling" << endl;
   output << "CUT:N 2J 0                                    $neutron cutoff" << endl;
   output << "CUT:A J 0.01 0                                  $alpha cutoff" << endl;
   output << "CUT:T J 0.01 0                                  $triton cutoff" << endl;
   output << "NPS 1E6                              $run for X neutron histories" << endl;
   output << "c STOP F18 0.01        $stop sim when all bins in tally F28 are RE 0.01 or less" << endl;
   output << "c PRDMP 5E4                             $print out every 5E4 histories" << endl;
   output << "c ----------" << endl;
   output << "c                        Tally Cards" << endl;
```

```
    output << "c _____"
<< endl;
    output << "F18:T,A,E,P  10                                  $Comb TA tally" << endl;
    output << "E18 0 0.3 5                                $energy bins for comb TA tally" << endl;
    output << "F28:A    10                                      $Alpha tally" << endl;
    output << "E28 0 0.3 5                               $energy bins for comb alpha tally" << endl;
    output << "F38:T    10                                     $Triton tally" << endl;
    output << "E38 0 0.3 5                               $energy bins for comb triton tally" << endl;
    output << "c
==========" <<
endl;
    output << "c                          Material Cards" << endl;
    output << "c
==========" <<
endl;
    output << "c" << endl;
    output << "c ////////////////////////////////////////////////////////////////////////" << endl;
    output << "c                 LiF   rho= 2.546 g/cc    95pct_wt Li6 Enrichment" << endl;
    output << "c ////////////////////////////////////////////////////////////////////////" << endl;
    output << "m1      3006    0.95" << endl;
    output << "        3007    0.05" << endl;
    output << "        9018    1" << endl;
    output << "c" << endl;
    output << "c ////////////////////////////////////////////////////////////////////////" << endl;
    output << "c               Metallic-Li   rho= 0.46682 g/cc    95pct_wt Li6 Enrichment" << endl;
    output << "c ////////////////////////////////////////////////////////////////////////" << endl;
    output << "m2      3006    0.95" << endl;
    output << "        3007    0.05" << endl;
    output << "c" << endl;
    output << "c ////////////////////////////////////////////////////////////////////////" << endl;
    output << "c                LiCl   rho= 2.025464 g/cc    95pct_wt Li6 Enrichment" << endl;
    output << "c ////////////////////////////////////////////////////////////////////////" << endl;
    output << "m3      3006    0.95" << endl;
    output << "        3007    0.05" << endl;
    output << "        17035   0.75770" << endl;
    output << "        17037   0.24230" << endl;
    output << "c" << endl;
    output << "c ////////////////////////////////////////////////////////////////////////" << endl;
    output << "c               LiOH   rho= 1.406227313 g/cc    95pct_wt Li6 Enrichment" << endl;
    output << "c ////////////////////////////////////////////////////////////////////////" << endl;
    output << "c" << endl;
    output << "m4      1001    1" << endl;
    output << "        3006    0.95" << endl;
    output << "        3007    0.05" << endl;
    output << "        8016    1" << endl;
    output << " c" << endl;
    output << "c ////////////////////////////////////////////////////////////////////////" << endl;
    output << "c               LiBr   rho= 3.429046674 g/cc    95pct_wt Li6 Enrichment" << endl;
    output << "c ////////////////////////////////////////////////////////////////////////" << endl;
    output << "c" << endl;
    output << "m5      3006    0.95" << endl;
    output << "        3007    0.05" << endl;
    output << "        35079   0.5069" << endl;
    output << "        35081   0.4931" << endl;
    output << "c" << endl;
    output << "c ////////////////////////////////////////////////////////////////////////" << endl;
```

```
    output << "c               Li3N   rho= 1.174173185 g/cc    95pct_wt Li6 Enrichment" << endl;
    output << "c ////////////////////////////////////////////////////////////////////////////" << endl;
    output << "c" << endl;
    output << "m6      3006    2.85" << endl;
    output << "        3007    0.15" << endl;
    output << "        7014    1" << endl;
    output << "c" << endl;
    output << "c ////////////////////////////////////////////////////////////////////////////" << endl;
    output << "c               LiI   rho= 4.049191185 g/cc    95pct_wt Li6 Enrichment" << endl;
    output << "c ////////////////////////////////////////////////////////////////////////////" << endl;
    output << "c" << endl;
    output << "m7      3006    0.95" << endl;
    output << "        3007    0.05" << endl;
    output << "        53127   1" << endl;
    output << "c" << endl;
    output << "c ////////////////////////////////////////////////////////////////////////////" << endl;
    output << "c               Li2O2   rho= 2.221346057 g/cc    95pct_wt Li6 Enrichment" << endl;
    output << "c ////////////////////////////////////////////////////////////////////////////" << endl;
    output << "c" << endl;
    output << "m8      3006    0.95" << endl;
    output << "        3007    0.05" << endl;
    output << "        8016    1" << endl;
    output << "c" << endl;
    output << "c ////////////////////////////////////////////////////////////////////////////" << endl;
    output << "c                 Si   rho= 2.329 g/cc    95pct_wt Li6 Enrichment" << endl;
    output << "c ////////////////////////////////////////////////////////////////////////////" << endl;
    output << "m100    14028.70c   922" << endl;
    output << "        14029.70c   47" << endl;
    output << "        14030.70c   31" << endl;
    output.close();
}



int main()
{



    ifstream mat_den_input;
    mat_den_input.open("density_material_index.txt");
    int i = 1;

    bool grab_data;

    bool make_new = 0;
    if (make_new) {
        grab_data = FALSE;
    }
    else
        grab_data = TRUE;


    if (make_new) {
        for (int b = 1; b <= 8; b++) {
            for (int a = 1; a <= 20; a++) {
```

```
            // get new material number and density to input into input-file-writing function
            getline(mat_den_input, mat_den);

            // use index value i to create file names for input and output files
            name.append(to_string(i));
            name.append(".txt");
            out.append(to_string(i));
            out.append("_output.txt");

            // create input file
            // write_new_singlecell_inputfile(mat_den, name);
            write_new_xdsmsnd_inputfile(mat_den, name);


            // clear strings for use on next loop iteration
            name.clear();
            mat_den.clear();
            out.clear();
            i++;
        }
    }
}

if (grab_data) {

    ofstream results_alpha;
    results_alpha.open("results_alpha.csv");
    ofstream results_alpha_error;
    results_alpha_error.open("results_alpha_error.csv");
    ofstream results_triton;
    results_triton.open("results_triton.csv");
    ofstream results_triton_error;
    results_triton_error.open("results_triton_error.csv");
    ofstream results_comb;
    results_comb.open("results_comb.csv");
    ofstream results_comb_error;
    results_comb_error.open("results_comb_error.csv");

    // reset int i to 1 for index within loop
    i = 1;

    // use index value to pull strings/data from output files
    for (int b = 1; b <= 8; b++) {
        for (int a = 1; a <= 20; a++) {

            // use index value to determine output file name for reading
            out.append(to_string(i));
            out.append("_output.txt");

            // open output file
            ifstream mcnp;
            mcnp.open(out);
```

```
            // locate specified tallies from output file and save line as string within 2d string array
            cout << "Searching within file: " << i << endl;
            //alpha_holder[a - 1][b - 1] = datafinder(18, mcnp, 7);
            alpha_holder[a - 1][b - 1] = datafinder(28, mcnp, 14);
            cout << "alpha data found\n";
            //triton_holder[a - 1][b - 1] = datafinder(28, mcnp, 7);
            triton_holder[a - 1][b - 1] = datafinder(38, mcnp, 14);
            cout << "triton data found\n";
            //comb_holder[a - 1][b - 1] = datafinder(38, mcnp, 7);
            comb_holder[a - 1][b - 1] = datafinder(18, mcnp, 14);
            cout << "combo data found\n";
            i++;
            mcnp.close();
            out.clear();
         }
      }

      // parse data from string previously pulled from output files
      for (int a = 1; a <= 20; a++) {
         for (int b = 1; b <= 8; b++) {

            bucket_data = alpha_holder[a - 1][b - 1];
            results_alpha << bucket_data.substr(17, 11) << "\t";
            results_alpha_error << bucket_data.substr(29, 6) << "\t";
            bucket_data = triton_holder[a - 1][b - 1];
            results_triton << bucket_data.substr(17, 11) << "\t";
            results_triton_error << bucket_data.substr(29, 6) << "\t";
            bucket_data = comb_holder[a - 1][b - 1];
            results_comb << bucket_data.substr(17, 11) << "\t";
            results_comb_error << bucket_data.substr(29, 6) << "\t";
         }

         // end lines within output for CSV-friendly format
         results_alpha << endl;
         results_alpha_error << endl;
         results_triton << endl;
         results_triton_error << endl;
         results_comb << endl;
         results_comb_error << endl;
      }


      // close remaining files to clear memory
      mat_den_input.close();
      results_alpha.close();
      results_triton.close();
      results_comb.close();
      results_alpha_error.close();
      results_triton_error.close();
      results_comb_error.close();
   }
   return 0;
}
```